NAVAL POSTGRADUATE SCHOOL

MONTEREY, CALIFORNIA

THESIS

DEVELOPMENT OF AlGaN/GaN HIGH ELECTRON MOBILITY TRANSISTORS (HEMTS) ON DIAMOND SUBSTRATES

by

Wesley Scott Newham

June 2006

Thesis Advisor:	Todd R. Weatherford
Second Reader:	Andrew A. Parker

Approved for public release; distribution is unlimited

THIS PAGE INTENTIONALLY LEFT BLANK

REPORT DOCUMENTATION PAGE			Form Approved OMB No. 0704-0188
Public reporting burden for this collection of information is estimated to average 1 hour per response, including the time for reviewing instruction, searching existing data sources, gathering and maintaining the data needed, and completing and reviewing the collection of information. Send comments regarding this burden estimate or any other aspect of this collection of information, including suggestions for reducing this burden, to Washington headquarters Services, Directorate for Information Operations and Reports, 1215 Jefferson Davis Highway, Suite 1204, Arlington, VA 22202-4302, and to the Office of Management and Budget, Paperwork Reduction Project (0704-0188) Washington DC 20503.			
1. AGENCY USE ONLY *(Leave blank)*	**2. REPORT DATE** June 2006	**3. REPORT TYPE AND DATES COVERED** Master's Thesis	
4. TITLE AND SUBTITLE: Development of AlGaN/GaN High Electron Mobility Transistors (HEMTs) on Diamond Substrates			**5. FUNDING NUMBERS**
6. AUTHOR(S) Wesley Scott Newham			
7. PERFORMING ORGANIZATION NAME(S) AND ADDRESS(ES) Naval Postgraduate School Monterey, CA 93943-5000			**8. PERFORMING ORGANIZATION REPORT NUMBER**
9. SPONSORING /MONITORING AGENCY NAME(S) AND ADDRESS(ES) N/A			**10. SPONSORING/MONITORING AGENCY REPORT NUMBER**
11. SUPPLEMENTARY NOTES The views expressed in this thesis are those of the author and do not reflect the official policy or position of the Department of Defense or the U.S. Government.			
12a. DISTRIBUTION / AVAILABILITY STATEMENT Approved for public release; distribution is unlimited			**12b. DISTRIBUTION CODE**

13. ABSTRACT (maximum 200 words)

Silicon based semiconductor devices are rapidly approaching the theoretical limit of operation and are becoming unsuitable for future military requirements. The scope of semiconductor devices has been expanded by wide bandgap devices such as gallium nitride (GaN) to include the possibility for high power and high frequency operation. A new generation of high speed – high frequency devices is required to meet current and future military needs. The Gallium Nitride High Electron Mobility Transistor (HEMT) is showing great promise as the enabling technology in the development of military radar systems, electronic surveillance systems, communications systems and high voltage power systems. Typically, sapphire or silicon carbide is utilized as the substrate material in most HEMT designs. This thesis explores the possibility of utilizing a diamond substrate to increase the power handling capability of the AlGaN/GaN HEMT. Diamond offers increased thermal property parameters that can be simulated in the commercially available Silvaco software package. A complete electrical and thermal analysis of the model was conducted and compared to actual device characteristics. The results of the software simulation and measurements on the test devices indicate diamond substrates will enable the HEMT to be operated at a higher power than traditional sapphire substrate HEMTS.

14. SUBJECT TERMS High Electron Mobility Transistor, HEMT, Gallium Nitride, Heterostructure, Sapphire Substrate, Diamond Substrate, Silvaco, ATLAS, BLAZE, GIGA			**15. NUMBER OF PAGES** 75 **16. PRICE CODE**
17. SECURITY CLASSIFICATION OF REPORT Unclassified	**18. SECURITY CLASSIFICATION OF THIS PAGE** Unclassified	**19. SECURITY CLASSIFICATION OF ABSTRACT** Unclassified	**20. LIMITATION OF ABSTRACT** UL

NSN 7540-01-280-5500 Standard Form 298 (Rev. 2-89)
Prescribed by ANSI Std. 239-18

THIS PAGE INTENTIONALLY LEFT BLANK

Approved for public release; distribution is unlimited

DEVELOPMENT OF AlGaN/GaN HIGH ELECTRON MOBILITY TRANSISTORS ON DIAMOND SUBSTRATES

Wesley S. Newham
Lieutenant, United States Navy
BSEE, Auburn University, 2000

Submitted in partial fulfillment of the
requirements for the degree of

MASTER OF SCIENCE IN ELECTRICAL ENGINEERING

from the

NAVAL POSTGRADUATE SCHOOL
June 2006

Author: Wesley Scott Newham

Approved by: Todd R. Weatherford
Thesis Advisor

Andrew A. Parker
Second Reader

Jeffrey B. Knorr
Chairman, Department of Electrical and Computer Engineering

THIS PAGE INTENTIONALLY LEFT BLANK

ABSTRACT

Silicon based semiconductor devices are rapidly approaching the theoretical limit of operation and are becoming unsuitable for future military requirements. The scope of semiconductor devices has been expanded by wide bandgap devices such as gallium nitride (GaN) to include the possibility for high power and high frequency operation. A new generation of high speed – high frequency devices is required to meet current and future military needs. The Gallium Nitride High Electron Mobility Transistor (HEMT) is showing great promise as the enabling technology in the development of military radar systems, electronic surveillance systems, communications systems and high voltage power systems. Typically, sapphire or silicon carbide is utilized as the substrate material in most HEMT designs. This thesis explores the possibility of utilizing a diamond substrate to increase the power handling capability of the AlGaN/GaN HEMT. Diamond offers increased thermal property parameters that can be simulated in the commercially available Silvaco software package. A complete electrical and thermal analysis of the model was conducted and compared to actual device characteristics. The results of the software simulation and measurements on the test devices indicate diamond substrates will enable the HEMT to be operated at a higher power than traditional sapphire substrate HEMTS.

THIS PAGE INTENTIONALLY LEFT BLANK

TABLE OF CONTENTS

LIST OF FIGURES

THIS PAGE INTENTIONALLY LEFT BLANK

LIST OF TABLES

THIS PAGE INTENTIONALLY LEFT BLANK

ACKNOWLEDGMENTS

I can never express my gratitude enough to the people who have helped me complete this thesis. First I would like to thank Professor Todd Weatherford who provided me with necessary tools to complete this thesis. Your ability to make complex theories understandable was remarkable and made the design process easier. Thank you for keeping me focused and pulling me out of the weeds when I needed it. I would also like to thank Andrew Parker who was the second reader of this thesis. Your suggestions were thought provoking and added to the quality of this thesis.

I would like to thank Dr. Petra Specht from UC Berkeley for providing the GaN HEMT devices for testing. Your willingness to provide suggestions and guidance has enhanced the quality of this thesis.

I would like to thank my three children Josh, Sydney, and Chase. You guys have been a blessing to me and helped me in ways you will never know. You three always make me realize what the true meaning of life is. Thank you for being you.

To my wife, Rachel, thank you for always being the calm in the storm I have put us through during this process. You were always there and willing to assist every step of the way. I count my blessings every day and thank God that he has provided such a wonderful person for me to spend the rest of my life with. You inspire me everyday! Thank you!

THIS PAGE INTENTIONALLY LEFT BLANK

EXECUTIVE SUMMARY

Current AlGaN/GaN High Electron Mobility Transistors (HEMTs) grown on sapphire substrates have a low reliability due to thermal effects. The need for a reliable high-frequency, high-power HEMT device is necessary for future naval communication and radar needs. A computer model of an AlGaN/GaN HEMT has been developed for the purpose of studying the thermal effects due to self heating. The thermal effects were examined on a device grown on a sapphire substrate and then on a diamond substrate to determine if the high thermal conductivity parameter of diamond would provide a reduced device operating temperature. The model developed in this thesis was created with the commercially available Silvaco software package and includes the BLAZÉ™ heterojunction routine, the GIGA™ thermal modeling routine, as well as various models to simulate the low field mobility as a function of doping and lattice temperature.

The ATLAS™ model was created based on the parameters extracted from an actual AlGaN/GaN HEMT grown on a sapphire substrate. The parameters extracted from the actual device were utilized as baseline for the model development.

One of the critical parameters necessary to simulate heterojunction devices is polarization. The polarization effects present in heterojunction devices are spontaneous polarization and the piezoelectric effect and are crucial in the formation of the unique two dimensional electron gas (2DEG) channel present in heterojunction devices. Although ATLAS™ provides models to simulate the effects individually, the results were less than desirable. In the NPS model, an interface charge was placed on the AlGaN side of the heterojunction to simulate the polarization effects. This interface charge provided the necessary electron concentration to form the 2DEG which forms an abrupt bangap shift at the interface. This abrupt change forms a quantum well which induces the 2DEG to form. All parameters extracted from the physical model were able to be re-created in the software model to a high degree of accuracy.

Simulations were conducted utilizing a sapphire substrate to match the operational parameters of the physical device. Once an accurate model was developed, the substrate material was changed to diamond, and the thermal characteristics were studied. A

simulation of the sapphire substrate device and the diamond substrate device was conducted to determine if a change in the thermal parameters affected the device heating. The sapphire substrate HEMT model was validated with measurements over a temperature range of 27^0C (room temperature) to 300^0C. The validated device modeling then showed a dramatic change in the lattice temperature as well as the channel temperature of the device when the substrate was changed to diamond. The diamond substrate reduced the peak temperature of the device by 1/2 while the average channel temperature was reduced by 1/3.

The work presented in this thesis represents the most accurate NPS HEMT model developed to date and can be utilized in follow-on efforts to study reliability and high frequency operations. AlGaN/GaN HEMT is showing great promise in becoming the enabling technology in high-power, high-frequency semiconductor amplifiers, and the results of this thesis indicates that utilizing a diamond substrate will enhance the operation of the HEMT.

I. INTRODUCTION

The purpose of this thesis was to create an accurate electrical and thermal computer model of an AlGaN/GaN HEMT device in order to investigate device operating parameters as the substrate thickness and material are changed. To develop an accurate model, an actual AlGaN/GaN HEMT device was examined and parameters extracted utilizing Silvaco's UTMOST™ program. The biggest departure of this thesis compared to previous work in this area is that this work was based and verified with physical devices and correlated with simulated models. The data extracted from the physical device served as a benchmark in the development of the device model. The AlGaN/GaN HEMT model was created utilizing Silvaco's ATLAS™, BLAZE™, and GIGA™ routines.

This chapter will discuss the background that motivated this thesis, current uses of HEMT devices, the problems associated with HEMT devices, ongoing research and funding associated with HEMT research, and will conclude with a summary of previous results and problems encountered. Chapter two will describe HEMT device physics and operation. Chapter three will outline the procedures for testing the actual HEMT device, the Silvaco model design as well as the physics models utilized to match the model with the actual device, and compare the physical device characteristics with the model results. Finally, chapter four will conclude the thesis with conclusions and recommendations and discuss possible future research.

A. BACKGROUND

To achieve the vision of Sea Power 21, the United States Navy requires new technology in the field of high-power, high-frequency electronics to field new state of the art systems. Current silicon technology is not capable of achieving the performance required by future systems. The technology that is poised to fulfill the future needs of industry and the Navy is wide bandgap (WBG) semiconductor devices. In particular, the most promising device to satisfy many of the future needs of the Navy is the GaN High Electron Mobility Transistor (HEMT). Some desirable attributes of next generation WBG electronics include the ability to withstand currents in excess of 5 kA and voltages

in excess of 50 kV, provide rapid switching, maintain good thermal stability while operating at temperatures above 250° C, have small size and light weight, and be able to function without bulky heat-dissipating systems [1]. Table 1 provides a comparison of the various semiconductor technologies available today.

	Si (----)	GaAs (AlGaAs/ InGaAs)	InP (InAlAs/ InGaAs)	4H SiC (----)	GaN (AlGaN/ GaN)
Bandgap (eV)	1.1	1.42	1.35	3.26	3.49
Electron mobility (cm^2/Vs)	1500	8500	10000	700	900
Saturated (peak) electron velocity ($x10^7$ cm/s)	1	2.1	2.3	2	2.7
2DEG sheet electron density (cm^{-2})	NA	$<4 \times 10^{12}$	$<4 \times 10^{12}$	NA	$20x10^{12}$
Critical breakdown field (MV/cm)	0.3	0.4	0.5	2	3.3
Thermal conductivity (W/cm-K)	1.5	0.5	0.7	4.5	>1.7
Relative dielectric constant (εr)	11.8	12.8	12.5	10	9.0

Table 1: Electronic Properties of Semiconductor Materials [2]**.**

In addition to becoming the enabling technology for future systems, GaN HEMTs have the potential to replace vacuum tubes in high power millimeter wave radar and electronic warfare systems. They have the potential to deliver high power at high voltage and do it at a fraction of the cost of current vacuum tube technology. The wide bandgap of GaN increases the breakdown field by five times and the power density by a factor of 10 to 20 compared with GaAs based devices. This results in smaller components with less capacitance for the same operating power, which results in a wider range of bandwidth.

GaN HEMT devices appear to be a great technology on paper, and great progress is being made toward technology development and process improvement. There have been demonstrations of very high output power densities in GaN HEMTS, but significant developmental work remains. One of the remaining issues is reliability. The output power from these devices can permanently degrade over a relatively short period of time. A phenomenon known as current collapse, a reduction in the dc drain current, after the application of a high drain–source voltage is prevalent in many GaN HEMT devices.

The high voltage leads to the injection of hot carriers into regions of the device adjacent to the conduction channel that contains deep traps [3]. One reliability issue this thesis attempts to address is how increased thermal stress affects the operation of the GaN HEMT. It has been shown that the DC characteristics are better for HEMTs fabricated on SiC substrate than on a sapphire substrate, possibly because of the increased thermal conductivity of SiC. The model developed in this thesis will examine the DC characteristics of the HEMT utilizing a diamond substrate. Diamond's thermal conductivity is about twice that of SiC and, therefore, will reduce the channel temperature of the HEMT, which will increase the power density potential and reduce thermally induced reliability issues.

B. ALGAN/GAN HEMT RESEARCH

1. Defense Advanced Research Projects Agency (DARPA)/Microsystems Technology Office (MTO)

DARPA is currently funding many research projects dealing with WBG development and implementation. One DARPA program currently underway is the Wide Bandgap Semiconductor-Radio Frequency (WBGS-RF) program. The program objectives are:

- Develop reliable, high performance devices and MMICs with
  - Higher power
  - Superior thermal performance
  - Higher efficiency
- Rapid insertion into DoD RF systems.

The WBGS-RF program is organized into three phases. Phase I is complete and was focused on WBG semiconductor materials. The output of Phase I results in high quality Si and SiC substrates and highly uniform GaN epitaxy, utilizing both MBE and MOCVD. Phase II is scheduled for three years and is currently underway. Phase II is concerned with device technologies such as X and Q band discrete components. The output of Phase II will be device demonstrations. Phase III is a two-year phase concerned with electronic integration and circuit technologies.

The DARPA WBGS-RF program has been awarding contracts in the fields of wide bandgap materials optimization, wide bandgap device fabrication and modeling, high yield wide bandgap MMICs, and packaging and thermal management of wide bandgap devices. There were multiple contract awards starting in calendar year 2005 totaling $75-$110 million dollars.

2. DARPA Wide Bandgap Semiconductor Technology Initiative (WBGSTI)

Another project sponsored by DARPA that is dedicated to advancing WBG technology is the WBGSTI. The objectives of the WBGSTI program are to scale up high quality SiC substrates, develop alternative substrates, develop uniform AlGaN/GaN HEMTs, and to examine materials/device correlations. This project is unique because it has developed a Tri-Service team comprised of the Air Force Research Laboratory (AFRL), Army Research Laboratory (ARL), and the Naval Research Laboratory (NRL). The Tri-Service team is composed of a Materials Panel and a Device Panel. Figure 1 depicts the interaction of the Tri-Service team.

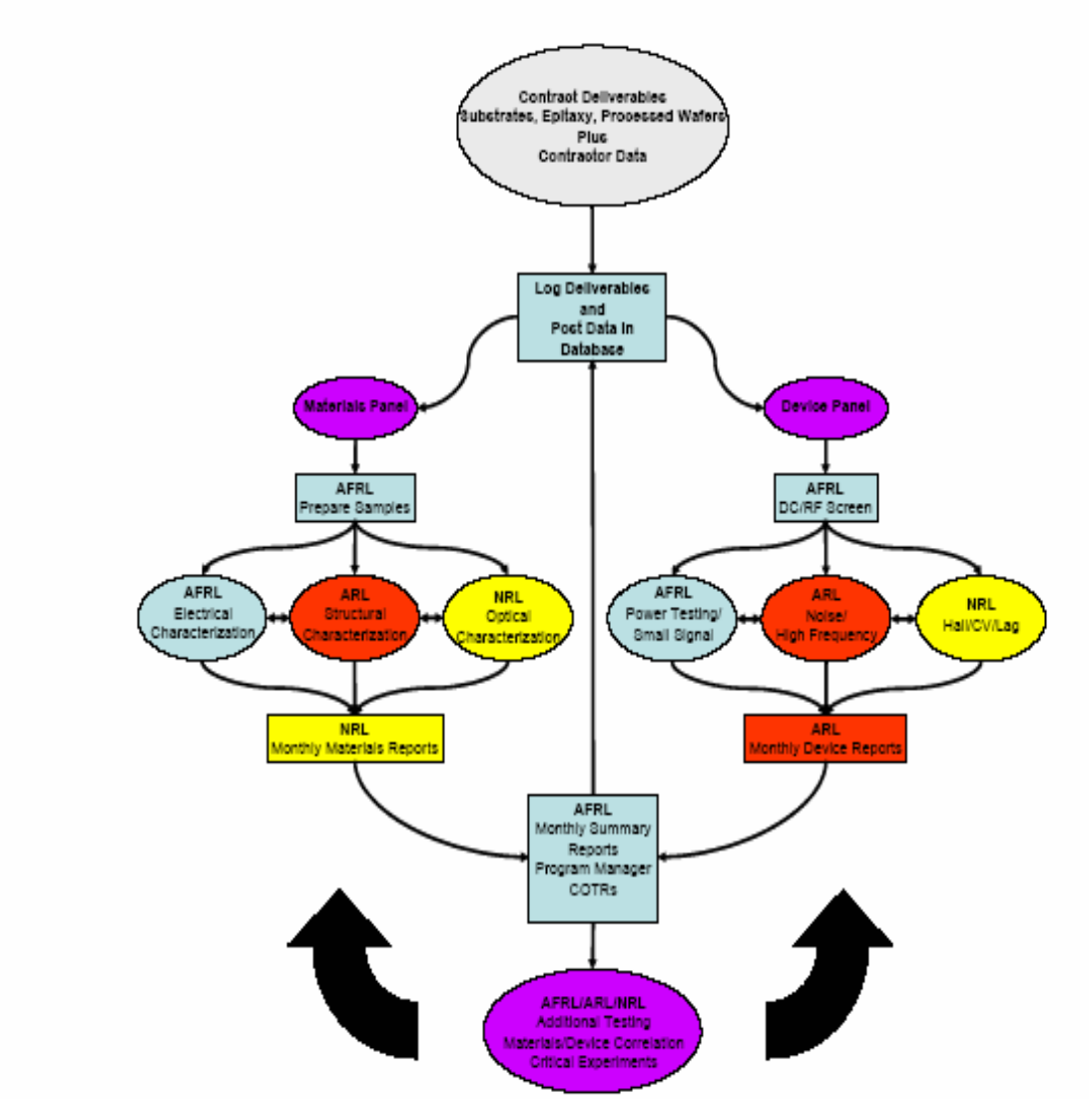

Figure 1: Tri-Service Team Interaction [4]**.**

The WBGSTI is a multi-phase, multi-year project that is poised to revolutionize the development of WBG devices. This project has the potential to change the way in which high-power, high-frequency systems are designed.

C. SUMMARY OF PREVIOUS RESEARCH

This section summarizes previous Naval Postgraduate School modeling attempts relating to AlGaN/GaN HEMT modeling research. The previous efforts by Eimers [5], Holmes [6], and Salm [7] concentrated on correctly modeling the HEMT device.

Previous versions of the Silvaco software did not provide adequate models for the surface charge or piezoelectric effects contained in AlGaN/GaN HEMTS. Therefore, many of the earlier attempts to correctly model the HEMT device were focused on independently developing these models to include in the Silvaco routine.

In [6], Holmes attempted to incorporate the polarization, piezoelectric and spontaneous effects into the HEMT model utilizing a C-interpreter method. Holmes was able to get an adequate I-V characteristic of a HEMT device utilizing a C-interpreter routine. However, his model needed to be refined to more closely match the overall operation of the HEMT device.

Since the completion of Holmes' thesis in 2002, Jon C. Freeman [8] developed a method to model GaN HEMTs with the Silvaco software package. In particular, he utilized ATLAS™ to add the effects of strain, piezoelectricity, and spontaneous polarization at the interfaces. The objectives of Holmes' thesis seem to have been met by Silvaco's software upgrade and Freeman's research. The model developed in this thesis incorporated the new Silvaco models and resulted in a more accurate device model.

Salm's [7] thesis, was the first Naval Postgraduate School attempt to utilize the piezoelectric model developed by Silvaco in a HEMT device simulation. Although he was not able to get accurate results with the piezoelectric model, he modeled the effect with an interface charge, and his results were adequate and more accurately modeled the desired characteristics of a HEMT device. His thesis also studied the thermal characteristics of the device utilizing the GIGA™ module. The GIGA™ module is capable of giving a numerical, as well as illustrative, representation of device heating. Salm's results indicated a remarkable difference in device heating due to a change in substrate material. The specifics of the structure and device physics will be discussed in chapter three of this thesis.

II. HIGH ELECTRON MOBILITY TRANSISTORS (HEMT)

This chapter presents an introduction to the High Electron Mobility Transistor (HEMT). The theory of operation for a HEMT device will be discussed to include equations, bandgap calculations, and the unique feature of the HEMT, the two dimensional electron gas (2-DEG). This chapter will conclude with an overview of the AlGaN/GaN structure designed and fabricated by the University of California at Berkeley.

A. HEMT FUNDAMENTALS

1. HEMT Structure

The GaN HEMT is similar to a typical MESFET in that it is a three terminal device that utilizes the gate to control current flow. The Naval Postgraduate School was provided with an array of devices designed and tested by Susie Tzeng [9] from the University of California at Berkeley. The exact structure dimensions shown in Figure 3 selected for this thesis includes a gate length (L_g) of 2µm, a gate width (W_g) of 100 µm, and a source to gate (L_{gs}) and gate to drain (L_{gd}) distance of 2 µm. Additionally, the Al (x) composition of the Berkeley HEMT was varied between 28% and 35%. The Al composition selected for this thesis was 28%. Figure 2 illustrates the layer structure of the device and Figure 3 defines the regions for the dimensions described above.

Figure 2: AlGaN/GaN HEMT Layer Structure.

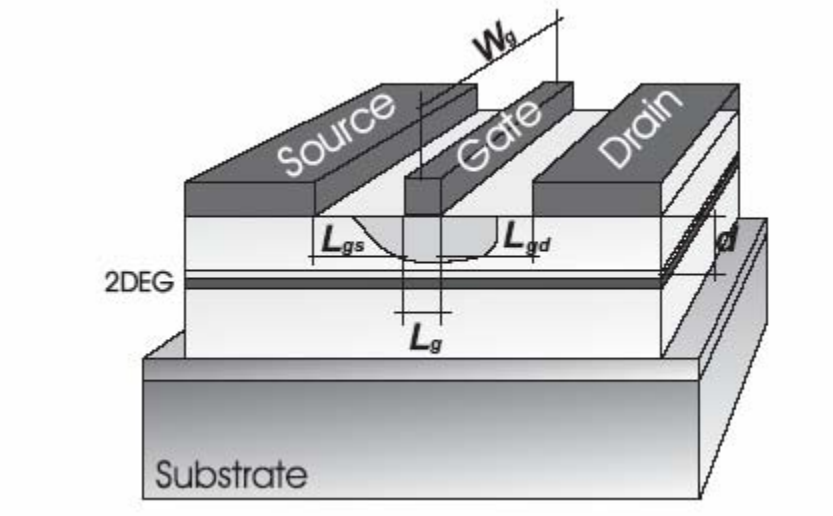

Figure 3: HEMT Device Dimensions [10]**.**

Ti/Al/Ni/Au ohmic metallization was deposited by e-beam evaporation and patterned by lift-off [9]. This process resulted in a contact resistance of approximately $5\times10^{-5}\Omega\text{-cm}^2$. The physical characteristics of the Berkeley device were utilized as an input to the ATLAS™ model and are discussed in chapter three of this thesis. Figure 4 is a scanning electron microscope (SEM) image of the HEMT device structure where the gate contact can be seen positioned between the source and drain ohmic contacts [9].

Although a complete strain analysis of the device is beyond the scope of this thesis, an overview of the strains and polarization effects in a HEMT device will be discussed in section two of this chapter. The polarization effects inherent in HEMT devices have been modeled by Dr. Jon Freeman [8] and can be incorporated utilizing the Silvaco software package. The modeling efforts of this thesis will be detailed in chapter three of this thesis to include the polarization effects that occur in HEMT devices.

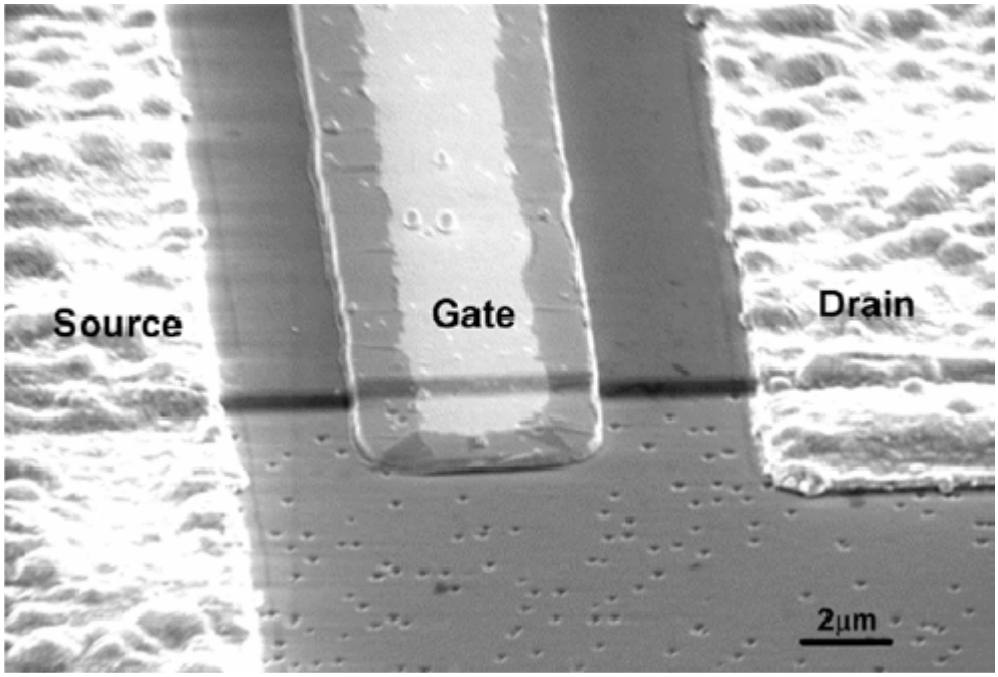

Figure 4: SEM Image of Berkeley GAN HEMT device. [9]**.**

2. AlGaN/GaN HEMT Fundamentals

The AlGaN/GaN HEMT also known as the modulation doped field effect transistor (MODFET) has similar DC characteristics to the MESFET. The unique feature of the HEMT is channel formation from carriers accumulated along a grossly asymmetric heterojunction, i.e. a junction between a heavily doped high bandgap and a lightly doped low bandgap region [1]. Instead of the channel being formed as in a standard homojunction device, a two dimensional electron gas (2DEG) is formed at the heterointerface. To achieve proper operation of the device, the barrier layer $Al_xGa_{1-x}N$ must be at a higher energy level than the conduction band of the GaN channel layer. This conduction band offset transfers electrons from the barrier layer to the channel layer. The electrons that are transferred are confined to a small region in the channel layer near the heterointerface. This layer is called the 2DEG and a defining characteristic of the HEMT. There are many factors that determine the quality of the 2DEG. The factors involved in the development of the 2DEG are type of substrate, growing method, and level of doping of the carrier supply layer [10]. Electron density and mobility are important factors when dealing with a 2DEG and a more detailed discussion of the 2DEG will be presented later in this chapter.

a. HEMT Equations

This section will outline basic HEMT parameters. The primary operating parameters dealing with high power HEMT operations are the transconductance (g_m), the 2DEG sheet charge concentration (n_s), the drain current (I_D), the threshold voltage (V_T), and the contact barrier height (ϕ_b).

The typical DC measurement to determine the operation of a HEMT is the drain current versus the voltage drain to source (I_D vs. V_{DS}) while the gate is swept from below cutoff to saturation. Figure 5 is an I_D vs. V_{DS} curve extracted from one of the Berkeley devices.

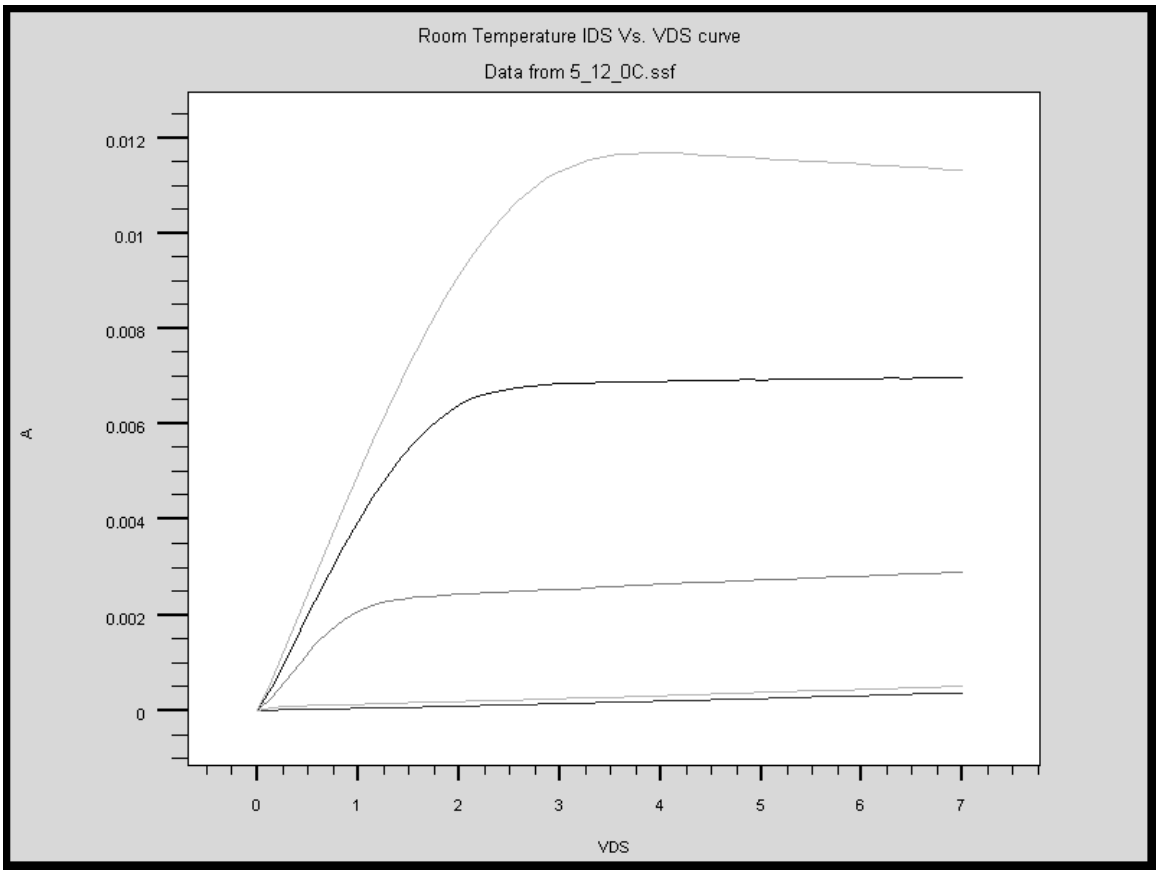

Figure 5: DC Output characteristic of AlGaN/GaN HEMT.

Unlike traditional MOS devices, the charge flowing in a HEMT device is normally confined to the 2DEG and changed by the gate voltage. When a gate voltage is applied to the device, the sheet charge concentration (n_s) is changed proportionally to gate voltage and is given by equation 2.1 [11]:

$$n_s = \frac{\varepsilon_i}{q(d_i + \Delta d)}\left(V_g - V_T\right) \tag{2.1}$$

where ε_i and d_i are the dielectric permeability and the thickness of the wide bandgap semiconductor, respectively, and Δd can be interpreted as the effective thickness of the 2DEG [11]. A typical n_s value for an AlGaN/GaN heterojunction is ~ 10^{13}/cm^2.

The threshold voltage is an important parameter because it is a measure of when the HEMT device will begin conducting. V_T can be expressed as:

$$V_T = \phi_B - \Delta E_C - \frac{qN_D}{2\varepsilon_i}d^2 \tag{2.2}$$

where ϕ_B is the gate Schottky-barrier height, and ΔE_C is the change in the conduction band at the heterojunction, and N_D is the background doping of the GaN layer.

Saturation current and transconductance are important measures of a HEMT device when utilized as a power amplifier. For long channel devices (L_g> 0.25μm), such as the ones presented in this thesis, I_{DSat} can be expressed the same as a standard MOSFET [9]:

$$I_{DSat} = \frac{\mu CW}{2L}(V_g - V_t)^2 \tag{2.3}$$

where μ is the carrier mobility, C is the gate capacitance, W is the gate width, and L is the gate length.

One of the measures of quality for a HEMT device is transconductance. It is a measure of how the drain current will change with a change in the gate voltage. Mathematically, transconductance is defined as [12]:

$$g_M = \left.\frac{\partial I_D}{\partial V_G}\right|_{V_{D=Constant}} = \frac{\mu C W}{L}(V_g - V_t). \quad (2.4)$$

Additionally, the output conductance known as the drain or channel conductance is an important measure in the HEMT device and is defined by [12]:

$$g_d = \left.\frac{\partial I_D}{\partial V_d}\right|_{V_{g=Constant}}. \quad (2.5)$$

The output conductance plays a crucial role in determining the output impedance matching properties of different stages of an amplifier.

The equations presented above are a good starting point for modeling the Berkeley HEMT device. However, there are many variables within the equations that will be modified to achieve a proper model of the device. There are a variety of models included in the Silvaco package that can be incorporated into the device definition, and when necessary a more detailed description of the chosen model will be provided.

b. HEMT Material Composition Issues

As mentioned above, the HEMT is a three terminal device where conduction is controlled by the gate voltage. The biggest operational difference between a HEMT and a traditional MOS device is that instead of creating a channel between the source and drain with a doped material, a wider bandgap material barrier layer ($Al_xGa_{1-x}N$) is grown on top of the channel and serves as a carrier supply layer [9]. Therefore, the channel is formed as a 2DEG below the doped layer which increases mobility due to a reduction in impurity scattering. A technique utilized to increase the electron density in the channel is to increase the Al mole fraction (x) in the $Al_xGa_{1-x}N$ layer. An increase in the Al mole fraction results in a higher bandgap and a larger conduction band discontinuity ΔE_C relative to the GaN [13]. The higher bandgap and ΔE_C results in an increase in the composite breakdown field and improves carrier confinement. Additionally, the piezoelectric and spontaneous polarization charges increase and serve to confine the carriers to the 2DEG. The effects of increasing the Al

mole concentration are attractive, but there is a limit to benefit gained. Figure 6 illustrates the electron density as a function of Al composition.

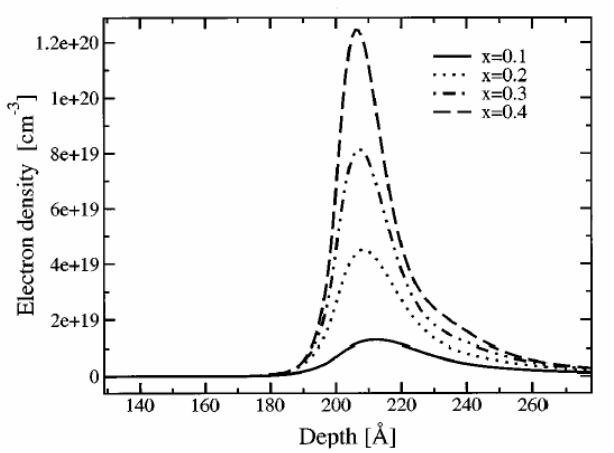

Figure 6: 2DEG electron density distribution for different Al(x) composition [14] **.**

Increasing the Al mole fraction also results in a reduced carrier mobility due to different effects including, intersubband scattering, increased alloy disordering in AlGaN, increased density of interface charges and larger potential fluctuations at the interface due to the surface roughness [14]. The Al composition for the device tested in this thesis is 28%, which roughly correlates to an electron density of 2e19 cm^{-3}.

c. HEMT Operational Parameters

This section will provide an overview of the device structure, where the 2DEG is created, and the energy bandgap diagrams of an AlGaN/GaN HEMT device.

The HEMT operational characteristics are based on the MESFET. The 2DEG is formed just below the heterojunction where the defects are lower and a higher electron mobility is possible. Figure 3 gives a visual estimate of where the 2DEG will be within the structure. The conductivity of the two dimensional channel is given by [10]:

$$\sigma = qn_s\mu \tag{2.6}$$

where q is the electron charge, n_s is the sheet carrier concentration given by equation 2.1, and μ is electron mobility.

Figure 7 depicts the typical bandgap diagram of an AlGaN/GaN HEMT device.

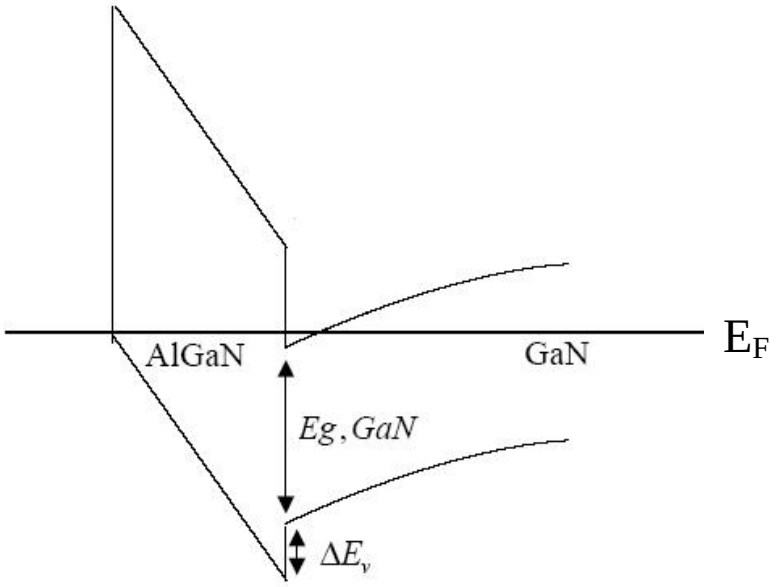

Figure 7: Bandgap diagram of AlGaN/GaN HEMT [9]**.**

One of the defining characteristic of a heterojunction device is the abrupt bandgap shift where the AlGaN layer meets the GaN Layer. The polarization effects that occur at this interface allows the 2DEG to be formed and become a conducting channel when properly biased.

The I_d vs. V_{ds} curve generated in Figure 5 will serve as the basis for discussion of the HEMT operating conditions. The initial values for the measurement were:

- Source voltage (V_s) =0
- Drain voltage (V_d) = 0
- Gate voltage(V_g)=-5

The source voltage was held constant and the drain voltage was swept from 0-7 V. The gate voltage began at -5 V and was incremented by 1 V per sweep to a final value of -1V. With the V_s and V_g = 0V, V_d was incremented in steps up to 7 V. It is apparent from

Figure 5 that a small current began to flow in the 2DEG channel with no gate voltage. By applying a positive voltage to the drain, current will flow due to the potential difference between the source and drain, but the magnitude of the current flow is controlled by the gate. Each branch in the diagram represents a 1 V increase in V_g which causes the drain-source current to increase linearly until the saturation point of the device is reached. The value of I_{Dsat} is dependant upon the n_s concentration. By increasing the concentration of n_s, the 2DEG is capable of transferring more charge from source to drain.

Unlike a typical MOS I_d vs. V_{ds} curve, GaN HEMTs on a sapphire substrate show a small negative slope in the saturation region. This anomaly is known as negative resistance and is attributed to self-heating of the device due to the poor thermal conductivity of sapphire[1].

3. Two Dimensional Electron Gas (2DEG)

The 2DEG in $Al_xGa_{1-x}N$/GaN based HEMT is induced by strong polarization effects [15]. Ambacher *et al*., utilizing piezoelectric constants obtained from previous research, calculated the induced sheet charge bound at the heterojunction interface. His conclusion was that the formation of the 2DEG in AlGaN/GaN structures was the result of both spontaneous polarization (P_{SP}) and the strain induced piezoelectric effects (P_{PE}) [15]. The Silvaco software package includes new modeling parameters that will enable a more realistic HEMT device model to be developed. The following sub-sections address the polarization effects of a GaN HEMT and will provide some of the variables that affect the 2DEG.

a. Spontaneous Polarization

The two distinct polarization mechanisms found in GaN HEMTs enable a high carrier concentration even though there may be no intentional doping. Spontaneous polarization is the effect that is present at the heterojunction even though there is no strain present. The spontaneous polarization (P_{SP}) is developed due to the wurtzite group III-nitrides being tetrahedrally coordinated with a lack of symmetry along the [0001] axis or c-direction [10]. The polarization effects vary according to the how the structure was formed. The structure will have either N-face or Ga-face surfaces. The Berkeley device

provided was grown on sapphire by MOCVD which results in Ga-faced structures only. Figure 8 shows the crystal structure of a wurtzite Ga-face.

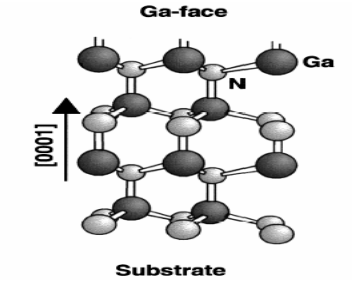

Figure 8: Schematic drawing of the crystal structure of wurtzite Ga-face[15]**.**

In the case of the wurtzite crystal grown in the manner previously discussed, the P_{SP} will be given as a constant determined by the method of growth. Table 3 provides the spontaneous polarization, piezoelectric and dielectric constants of AlN and GaN. Ambacher *et al*. [15] developed this table from many sources and utilized the constants to determine the P_{SP} and P_{PE} for an AlGaN/GaN structure.

wurtzite	AlN	GaN
P_{SP} [C/m^2]	−0.081	−0.029
	1.46	0.73
e_{33}	1.55	1
[C/m^2]		0.65
		0.44
e_{31}	−0.60	−0.49
[C/m^2]	−0.58	−0.36
		0.33
		−0.22
e_{15}	−0.48	−0.3
[C/m^2]		−0.33
		−0.22
ϵ_{11}	9.0	9.5
ϵ_{33}	10.7	10.4

Table 2: Spontaneous polarization, piezoelectric and dielectric constants of AlN, GaN [15]**.**

The ability to achieve a high carrier concentration at the 2DEG is determined by the ability of the structure to confine carriers through the polarization effects. To achieve a high carrier confinement, the polarization directions should be the same. The polarization induced sheet charge density (σ) should be positive. This positive sheet charge attracts electrons and forms the 2DEG. Figure 9 illustrates the polarization charge

effects for the different types of strain. The first case (a) where AlGaN (relaxed) is grown on top of GaN (relaxed), a positive sheet charge ($+\sigma$) is developed at the interface and a 2DEG forms. To enhance the polarization effects, example (b) grew tensile strained AlGaN over GaN which resulted in all polarization effects acting in the same direction. This also results in a positive sheet charge at the interface. The piezoelectric (P_{PE}) effects will be illustrated and calculated in the next section.

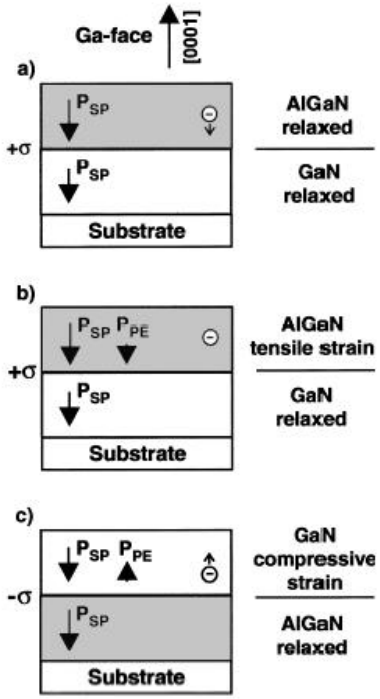

Figure 9: Ga-Faced polarization induced sheet charge density and directions for the spontaneous and piezoelectric polarization effects [15]**.**

b. Piezoelectric Polarization

The total polarization in the structure is given by $P_{SP} + P_{PE}=P_{TOTAL}$. Utilizing Table 2, the piezoelectric polarization can be calculated by the following equation given by [15]:

$$P_{PE} = e_{33}\varepsilon_z + e_{31}\left(\varepsilon_x + \varepsilon_y\right) \tag{2.7}$$

where a_0 and c_0 are the equilibrium values of the lattice parameters, $\varepsilon_z = \left(\frac{c - c_0}{c_0} \right)$ is the strain along the c-axis, and the in-plane strain $\varepsilon_x = \varepsilon_y = \left(\frac{a - a_0}{a_0} \right)$ is assumed to be isotropic. The third independent component of the piezoelectric tensor e_{15} is related to the polarization induced by shear strain, which is not applicable in this device. The relation between the lattice constants of the hexagonal GaN is given by Ambacher *et al*. [15] as:

$$\left(\frac{c - c_0}{c_0} \right) = -2 \left(\frac{C_{13}}{C_{33}} \right) \left(\frac{a - a_0}{a_0} \right) \tag{2.8}$$

where C_{13} and C_{33} are elastic constants provided in previous literature. The total piezoelectric polarization in the direction of the c-axis can be determined by equations 2.7 and 2.8 [15]:

$$P_{PE} = 2 \left(\frac{a - a_0}{a_0} \right) \left(e_{31} - e_{33} \left(\frac{C_{13}}{C_{33}} \right) \right). \tag{2.9}$$

Since the value of $\left[e_{31} - e_{33} \left(\frac{C_{13}}{C_{33}} \right) \right] < 0$ for AlGaN over the entire range of compositions, the piezoelectric polarization is negative for tensile and positive for compressive strained barriers, respectively [15]. GaN based semiconductors are attractive in HEMT designs due to the high piezoelectric constants. The piezoelectric fields developed in GaN devices can create a vertical electric field in the MV/cm range which increases the channel conductivity. Many of the polarization effects outlined above have been modeled into ATLAS™ as an upgrade to heterojunction modeling.

B. BERKELEY HEMT DESIGN

All HEMT structures provided to NPS were metal-organic chemical vapor deposition (MOCVD) grown by Emcore Corporation [9]. The structure was grown on [0001] c-plane sapphire substrate.

Figure 2 depicts the layer by layer structure of the device tested. From bottom to top, it consists of the sapphire layer, a buffer layer, 1.5 μm of unintentionally doped (UID) GaN, and approximately 25 nm of UID $Al_xGa_{1-x}N$. The Al composition, (x), in the Berkeley devices was varied between 28% and 35% to assess the impact of Al composition on the 2DEG transport properties and the device performance [9]. The GaN HEMT was fabricated by a 3-step process: dry-etch mesa isolation, ohmic contact metallization, and gate metallization. Figure 4 provides a SEM image of the device. Table 3 [9] shows the $Al_xGa_{1-x}N$ thickness as a function of the percent of Al.

Sample Number	Al%	$Al_xGa_{1-x}N$ thickness (Å)
1	28	267
2	29	230
3	30.2	230
4	32	221
5	34	242
6	35	206

Table 3 Al Composition and layer thickness of $Al_xGa_{1-x}N$ barrier layer in $Al_xGa_{1-x}N$/GaN HEMT structure [9]**.**

THIS PAGE INTENTIONALLY LEFT BLANK

III. AlGaN/GaN HEMT SILVACO MODEL

The model presented in this thesis was generated with Silvaco International's software package. An input deck was generated in the DECKBUILD™ VWF interactive tool, solved through the ATLAS™ routine, and analyzed utilizing the TONYPLOT™ tool. Additionally, the BLAZE™ routine, a routine specifically designed for group III-V materials and devices with position dependent band structures was utilized to simulate the AlGaN/GaN HEMT.

The desired result of this thesis was to generate an accurate HEMT model and determine the thermal characteristics of the device as the substrate thickness and material are changed. The GIGA™ routine was utilized to determine general thermal characteristics of the device. GIGA™ extends the ATLAS™ program to account for lattice heat flow and general thermal environments. The routing implements Wachutka's thermodynamically model of lattice heating which accounts for Joule heating, heating and cooling due to carrier generation and recombination, and the Peltier and Thomson effects [16].

The Silvaco software suite is a powerful simulation software that uses physics based simulations. Physically-based device simulators predict the electrical characteristics that are associated with specified physical structures and bias conditions. ATLAS™ achieves this simulation by applying a two or three dimensional grid that forms nodes throughout the structure. The nodes are solved in a matrix with charge transport equations from Maxwell's continuity and drift-diffusion equations [16].

The ATLAS™ simulator is a command driven simulator that requires an input in a specific sequence. The order in which the statements occur is important to the proper simulation of a device. There are five groups of statements, and if not correctly stated will result in errors or erroneous simulations. The required groups and statements are as follows [16]:

- Structure specification
    - Mesh
    - Region
    - Electrode
    - Doping
- Material Models Specification
    - Material
    - Models
    - Contact Interface
- Numerical Method Selection
    - Method
- Solution Specification
    - Log
    - Solve
    - Load
    - Save
- Results Analysis
    - Extract
    - TONYPLOT.

The above commands represent the entire structure definition and solution method. It is critical to have a firm understanding of the simulation variables prior to defining a structure. A small change in one variable or solution method can have undesirable consequences on device performance. Figure 10 depicts a flow chart of the device simulation utilizing Silvaco International's simulators and modules.

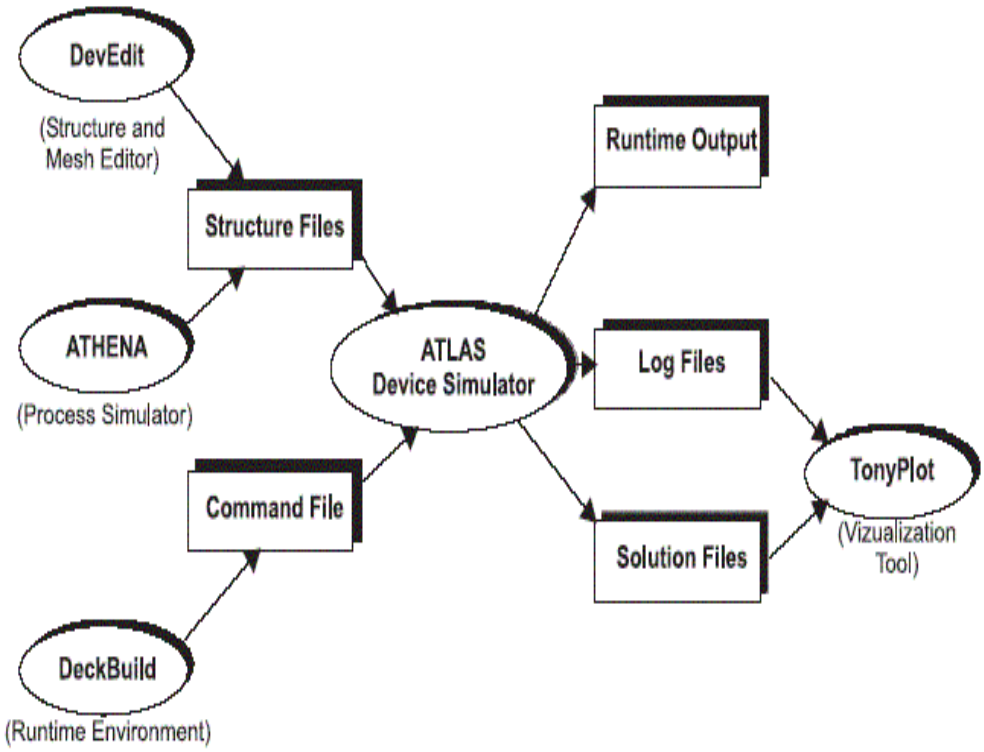

Figure 10: Silvaco Simulation Flowchart [16].

A. SILVACO SEMICONDUCTOR MODELING EQUATIONS

The models developed to simulate the operation of semiconductor devices consist of equations derived from Maxwell's laws, Poisson's equation, the continuity equations and the drift-diffusion transport equations [16]. The following sections discuss the equations in broad terms, and when necessary, a more detailed explanation of the equations will be presented.

The method in which the above equations will be solved is a prime consideration when developing a device model in ATLAS™. Several different numerical methods can be used for calculating the solutions to various device structures. Different solution methods are employed depending on the situation. The model developed in this thesis incorporated the lattice heating parameter simulated through GIGA™. When the lattice heating model is added to drift-diffusion equations an extra equation is added. The BLOCK algorithm solves the three drift diffusion equations as a Newton solution and follows this with a decoupled solution of the heat flow equations [16]. The NEWTON

algorithm solves all four equations in a coupled manner. NEWTON is preferred once the temperature is high, however BLOCK is quicker for low temperature gradients. The combination utilized for this thesis was: METHOD BLOCK NEWTON.

1. Poisson's Equation

Poisson's equation is a well known partial differential equation that has functions in electrostatics and theoretical physics. In semiconductor modeling it often serves as the starting point in obtaining quantitative solutions for electrostatic variables [12]. In electrostatics, Poisson's equation relates the electrostatic potential to the space charge density and is given by [16]:

$$\operatorname{div}\left(\varepsilon \nabla \Psi\right) = -\rho \tag{3.1}$$

where Ψ is the electrostatic potential, ε is the local permittivity, and ρ is the local space charge density. The local space charge density is a function of all mobile and fixed charges including electrons, holes, and impurities. The electric field is obtained from the gradient of the potential and is given by [16]:

$$\vec{E} = \nabla \Psi \tag{3.2}$$

2. Carrier Continuity Equations

The carrier continuity equations for electrons and holes are defined by [16]:

$$\frac{\partial n}{\partial t} = \frac{1}{q} \operatorname{div} \vec{J}_n + G_n - R_n \tag{3.3}$$

$$\frac{\partial p}{\partial t} = \frac{1}{q} \operatorname{div} \vec{J}_p + G_p - R_p \tag{3.4}$$

where n and p are the electron and hole concentration, $\vec{J}_n$ and $\vec{J}_p$ are the electron and hole current densities, G_n and G_p are the generation rates for electrons and holes, R_n and R_p are the recombination rates for electrons and holes and q is the magnitude of the charge on the electron. It is possible to solve for only the holes or electrons in the equations, and the model presented in this thesis solves the equations for electrons only. Hole transport in the HEMT is insignificant.

3. Transport Equations

Electrons in thermal equilibrium at temperature T_L within a semiconductor lattice obey Fermi-Dirac statistics. That is the probability f(ε) that an available electron state with energy ε is occupied by an electron is given by [16]:

$$f(\varepsilon) = \frac{1}{1 + \exp\left(\frac{\varepsilon - E_F}{kT_L}\right)} \tag{3.5}$$

where E_F is a spatially independent reference energy known as the Fermi level and k is the Boltzmann's constant. If $\varepsilon - E_F >> kT_L$, equation 4.5 can be approximated as:

$$f(\varepsilon) = \exp\left(\frac{E_F - \varepsilon}{KT_L}\right) \tag{3.6}$$

Statistics based on equation 3.6 are know as the Boltzmann statistics and were utilized in the formulation of the HEMT model. The current density equations know as the charge transport models are obtained by applying simplifications to the Boltzmann transport equation. These assumptions can result in a number of different transport models such as the drift-diffusion model, the energy balance model or the hydrodynamic model [16]. The choice of charge transport model will then have a major influence on the choice of generation and recombination model. The drift diffusion transport model was utilized in the development of this model. The following equations were derived in chapter three of [16], and show the conventional form of the drift-diffusion equation:

$$\vec{J}_n = qn\mu_n \vec{E}_n + qD_n \nabla n \tag{3.7}$$

$$\vec{J}_p = qp\mu_p \vec{E}_p + qD_p \nabla p \tag{3.8}$$

where D_n and D_p, in the case of the Boltzmann statistics corresponds to:

$$D_n = \frac{kT_L}{q}\mu_n \tag{3.9}$$

$$D_p = \frac{kT_L}{q}\mu_p . \tag{3.10}$$

4. Polarization Effects

Perhaps one of the most challenging aspects of modeling heterojunction devices in ATLAS™ is implementing the polarization effects present at the interface of the heterojunction. It has been widely published [15, 17] that surface donor like traps are the source of electrons in the channel and the polarization effects in AlGaN/GaN structures force the electrons into the channel. Previous modeling efforts have modeled the polarization effects as an interface charge of approximate $1e13\left(\frac{e}{cm^2}\right)$ at the heterojunction interface.

Recent upgrades to ATLAS™ include the ability to model polarization effects directly. The ATLAS™ polarization model was designed to simulate polarization in wurtzite materials and include spontaneous polarization and piezoelectric polarization. The model allows the designer to input the piezoelectric constants e_{31} and e_{33} as well as the elastic constants C_{13} and C_{33}. Various methods to implement the polarization model into the device model were attempted however, all attempts were unsuccessful. When incorporated into the model, the polarization effects were evident on the contour plots, but I was unable to get a representative bandgap diagram or I_d vs. V_d characteristic.

The polarization effects were modeled as an interface charge of approximately $1e13\left(\frac{e}{cm^2}\right)$ on the GaN side of the heterojunction. Ambacher *et al*. [15] utilizes the lattice constant (a), the piezoelectric constants (e), and the elastic constants (C) to derive the sheet concentration density in wurtzite materials. The sheet concentration density $\sigma(x)$ is given by :

$$\left|\sigma(x)\right| = \left|P_{PE}(Al_xGa_{1-x}N) + P_{SP}(Al_xGa_{1-x}N) - P_{SP}(GaN)\right|. \tag{3.11}$$

Substituting equation 2.9 for the P_{PE} variable gives:

$$\left|\sigma(x)\right| = \left|2\left(\frac{a(0)-a_0(x)}{a_0(x)}\right)\left\{e_{31}(x) - e_{33}(x)\left(\frac{C_{13}(x)}{C_{33}(x)}\right)\right\} + P_{SP}(x) - P_{SP}(0)\right|. \tag{3.12}$$

When the sheet charge density σ is divided by e, the result is the polarization induced sheet charge density. Figure 11 illustrates the induced sheet charge as a function of alloy composition (x).

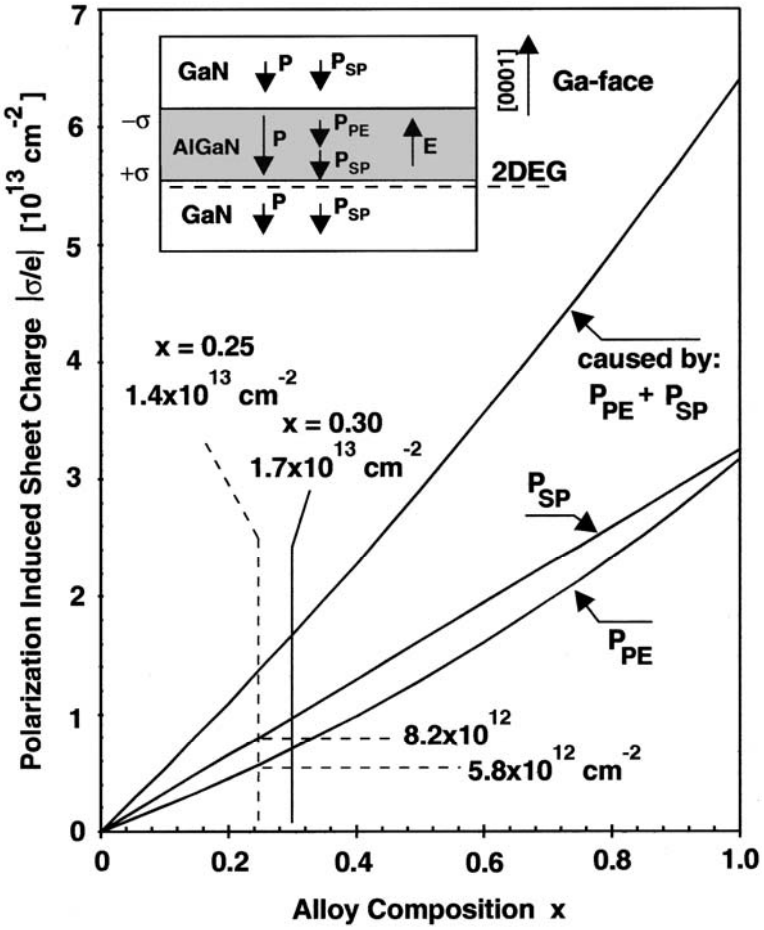

Figure 11: Sheet charge as a function of alloy composition [15]**.**

The device modeled in this thesis has an Al alloy content of 0.28, and a sheet charge of $0.99e^{13}$ cm^{-2} was introduced at the GaN side of the heterojunction to simulate the polarization effects.

Modeling the device in this manner resulted in a more realistic device model and allowed for continued thermal studies. When modeled with the interface charge, the HEMT device was characterized well, and with small discrepancies, matched the Berkeley devices. A comparison of the physical device in relation to the simulated device will be presented later in this chapter.

B. SILVACO MODEL

The model developed in ATLAS™ was designed based on the work of Tzeng [11]. The purpose of her dissertation was to study noise parameters in the HEMT device. The Naval Postgraduate School's purpose is to study the thermal characteristics of the device through measurements and a model developed in Silvaco to determine if a diamond substrate will enhance the thermal characteristics of the HEMT device. The following sections will contain a discussion of the modeling steps taken to simulate the HEMT device.

1. Model Definition

To develop the software model of the HEMT, ATLAS™ requires an input in the form of geometric statements to define the dimensions of the device to be modeled. The first step is to define the structure dimensionally and then assign a mesh to enclose the structure. The purpose of the mesh is to define solution points throughout the structure. Defining the mesh correctly is one of the most important factors in the model development. If the mesh is too coarse, the solutions will not be correct, and if the mesh is too finely defined, the computation time can be prohibitive. The rest of the program file is devoted to modifying statements and output parameters that will be discussed individually when necessary. The entire model definition file, referred to as a *.in file is provided in Appendix A. Figure 12 is a TONYPLOT™ structure view of the device modeled. The structure definition is saved in ATLAS™ as a *.str file. The graphic representing the HEMT device is a close up view in order to see the AlGaN layer. The actual device is 20μm thick. The structure file view in TONYPLOT™ provides a visual representation of the device performance. There are drop down menus that allow for a selection of the desired plot.

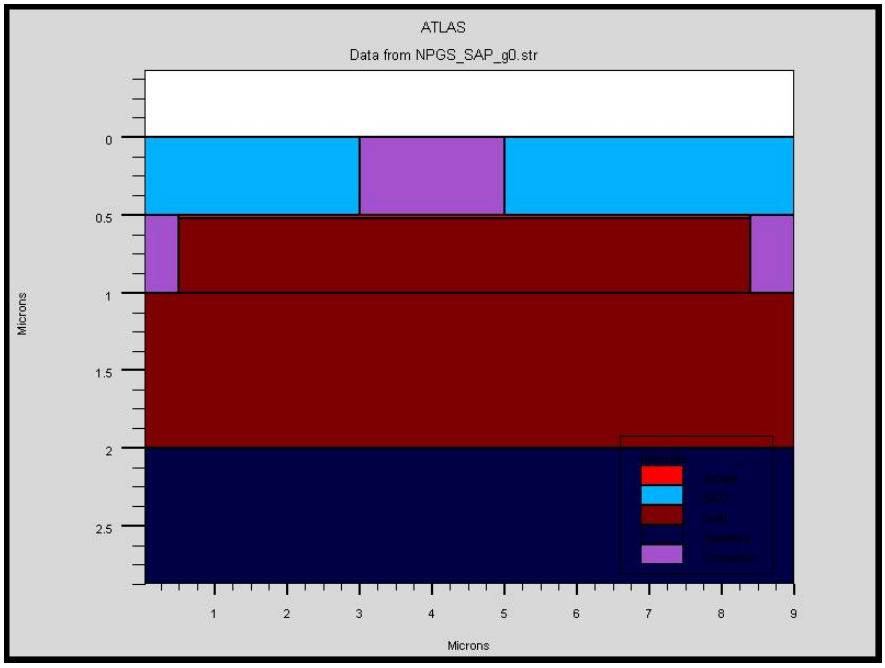

Figure 12: 2D Representation of the Modeled AlGaN/GaN HEMT.

2. Gate Characterization

The characterization of the gate was accomplished by measuring the gate leakage of the Berkeley device and then simulating the device. The gate on the HEMT is a Schottky barrier, and the characterization was accomplished by adjusting the gate workfunction until the leakage current on the simulation matched the measured values. Figure 13 (a) shows the simulated gate characteristic of the tested device and Figure 13 (b) shows the measured characteristic of the tested device.

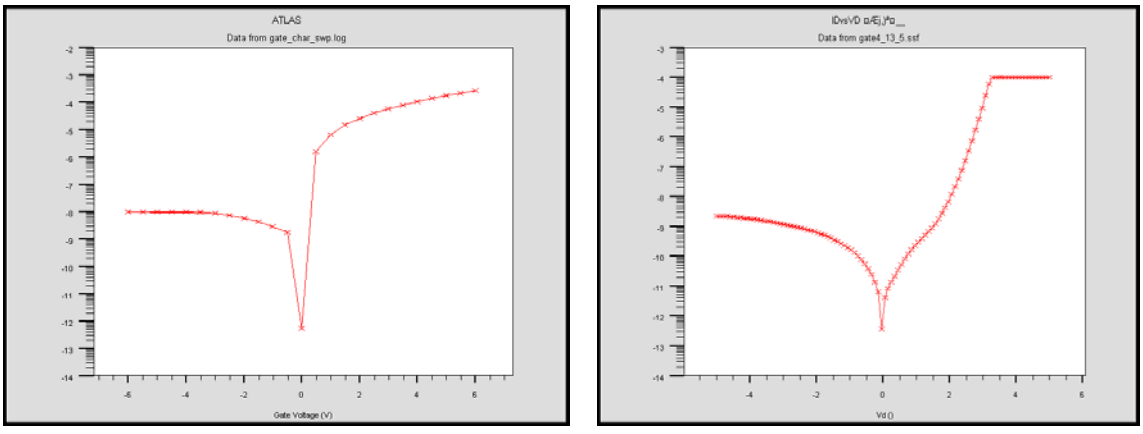

(a) **(b)**

Figure 13: (a) ATLAS™ Generated Gate Characterization and (b) Measured.

To test the device, the source and drain were set to 0V and the gate was swept from -6V to 6V. The simulated version matches the tested version with the exception of how low the current goes at V_{GS}=0. The difference is most likely due to the meshing technique used. Due to the magnitude of the current, is not a concern in the simulation. The simulated workfunction value of the Schottky gate that provided the best characterization was 4.3eV.

3. Heterojunction Bandgap Results

Simulating heterojunction devices in ATLAS™ is accomplished through BLAZE™, a compound material 2D simulator. BLAZE™ accounts for the effects of positionally dependent band structure by modifications to the charge transport equations [16]. The difference in the two bandgaps creates an abrupt discontinuity in the valence and conduction band. ATLAS™, through BLAZE™ provides three methods for defining the conduction band alignment for a heterojunction. The method utilized in this model is the ALIGN™ parameter. BLAZE™ allows the difference in the conduction band ΔE_C to be calculated by specifying the ALIGN parameter and the desired value of offset on the material statement. BLAZE™ creates the desired conduction band offset by modifying the electron affinity of the material for which the parameter is specified. The ALIGN parameter was set to 0.8 on the AlGaN layer which allowed 80% of the bandgap difference to appear as the conduction band discontinuity.

The 0.8 ALIGN parameter was established through previous HEMT design attempts [5, 7] and trial and error. Figure 14(a) shows the valence band characteristic with no bias, and Figure 14(b) shows the conduction band. The diagrams in Figure 14 are broken down into three regions. A cutline was utilized to extract the electrical properties from the compiled structure. The left region represents the gate electrode, the center region represents the AlGaN layer, and the right region is the GaN layer. The unique bandgap feature of the HEMT is evident at the AlGaN/GaN interface.

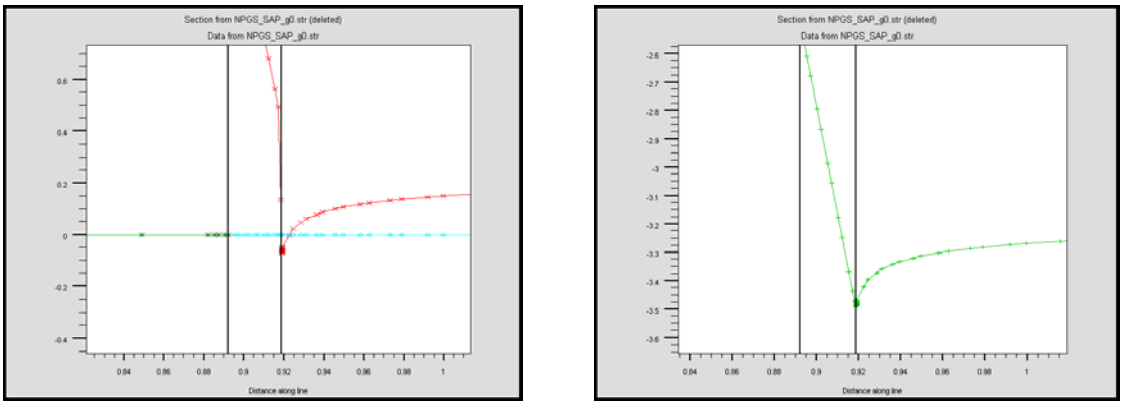

(a) (b)

Figure 14: Band diagram of HEMT showing (a) Conduction Band and (b) Valence Band.

Figure 15 is the full view of the bandgap diagram showing the conduction band in red, the Fermi level in blue and the valence band in green. The bandgap of the simulated structure was measured and found to be 3.42eV, the approximate value of GaN from Table 1. The value of this figure is that it shows the structure design is correct and that the 2DEG is formed on the GaN side of the heterojunction.

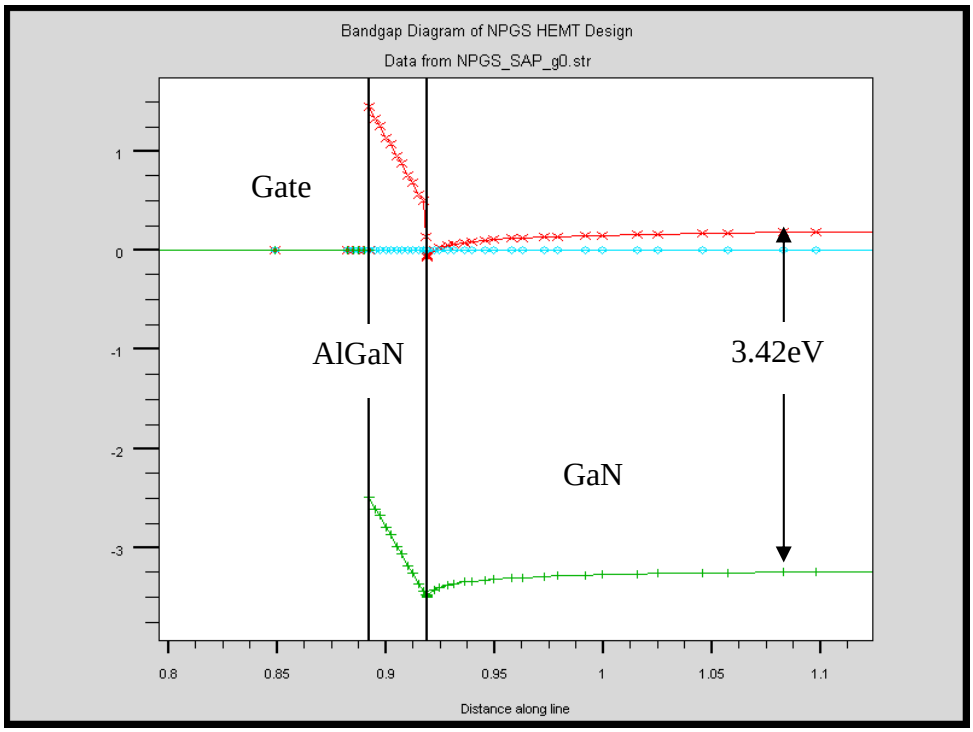

Figure 15: Band Diagram of modeled AlGaN/GaN HEMT.

4. Electron Concentration due to Polarization

Figure 15 clearly shows the effects of polarization at the heterojunction interface by the formation of the triangular shaped quantum well. The polarization charge causes the electron concentration to increase and a 2DEG is formed. As discussed in chapter II, a net positive polarization charge is present at the AlGaN/GaN junction in Ga-faced structures. Donor electrons will attempt to compensate this charge and will form the 2DEG that causes the conduction band to drop below the Fermi level at the interface. Figure 16(a) is a contour view of the structure that shows the electron concentration. The contour plot shows that there is a distinct 2DEG that has formed just below the AlGaN layer (the thin layer just below the gate electrode) as predicted. Figure 16(b) shows the cutline view of the electron concentration. The blue line is the electron concentration and the red line is the donor concentration. The increase of electrons to approximately $1e19\left(\frac{e}{cm^2}\right)$ from the background doping level of $1e15\left(\frac{e}{cm^2}\right)$ illustrates the effects of polarization and agrees with Ambacher's predictions[15].

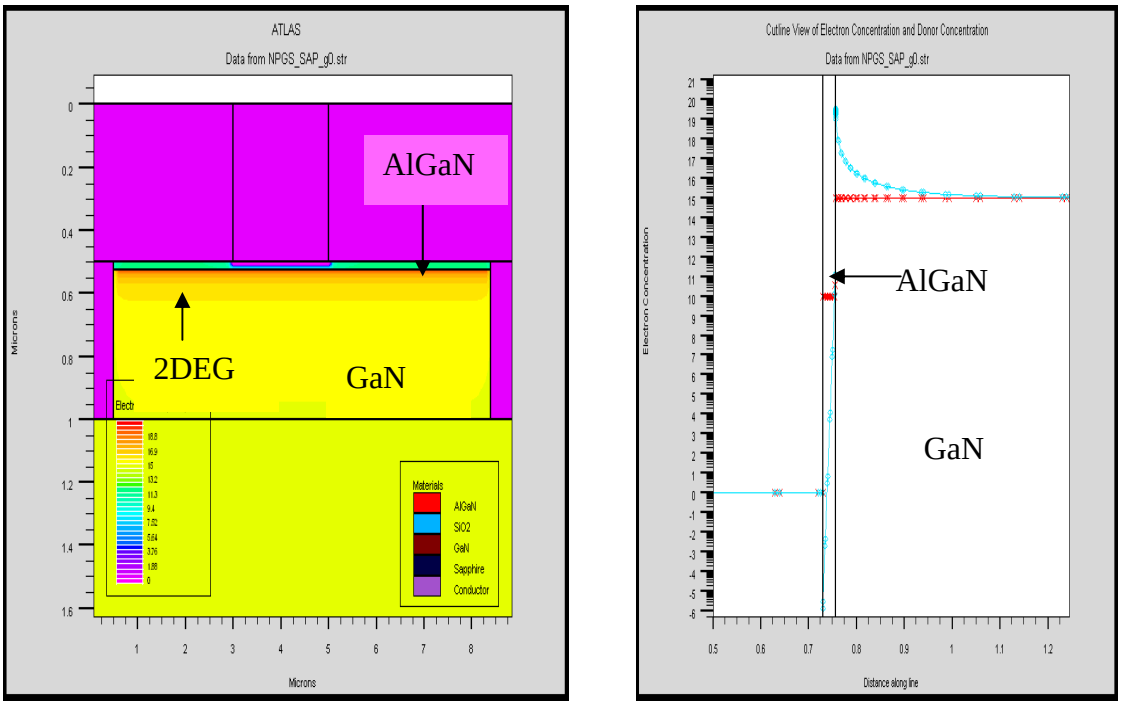

(a) (b)

Figure 16: Electron Concentration Contour View (a) and Cutline View (b).

5. I-V Curves

Once the model was complete and analyzed, a subroutine in ATLAS™ was created to generate the I_{ds} vs. V_{ds} (I-V) curves. The physical device provided by Berkeley was tested utilizing the UTMOST™ program and a Micromanipulator microscope probe system. The data extracted from the device was imported to TONYPLOT™ for analysis and comparison. The test performed on the model was performed with the same DC parameters that were utilized in the physical device testing. Figure 17 is the I-V characteristic of the HEMT model and Figure 18 is the I-V characteristic of the measured device.

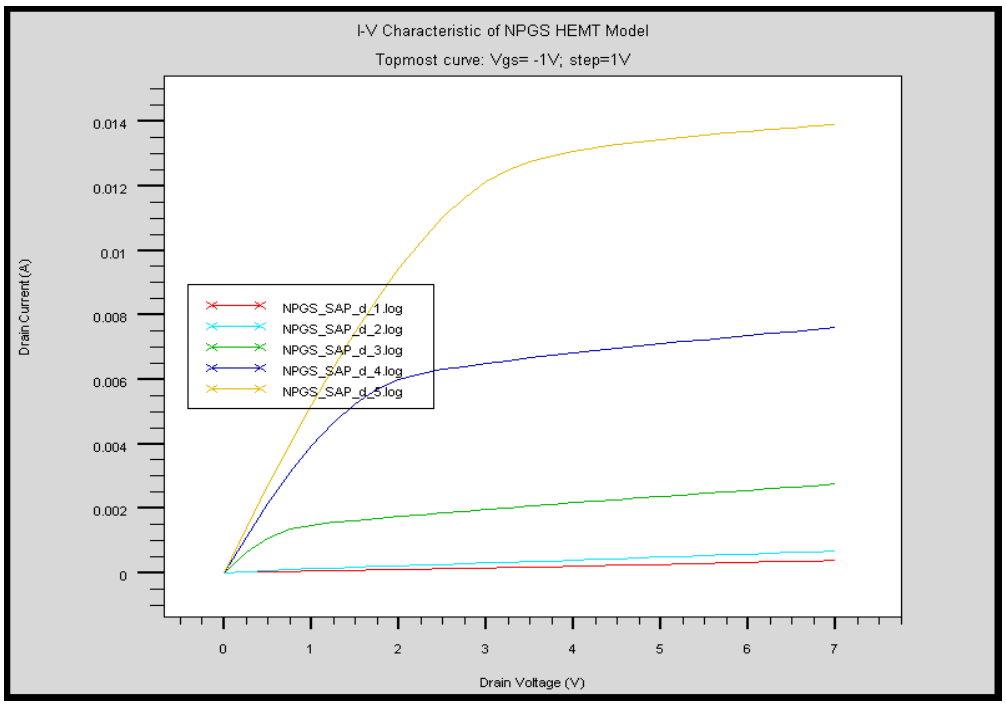

Figure 17: NPS HEMT Model I-V Characteristic.

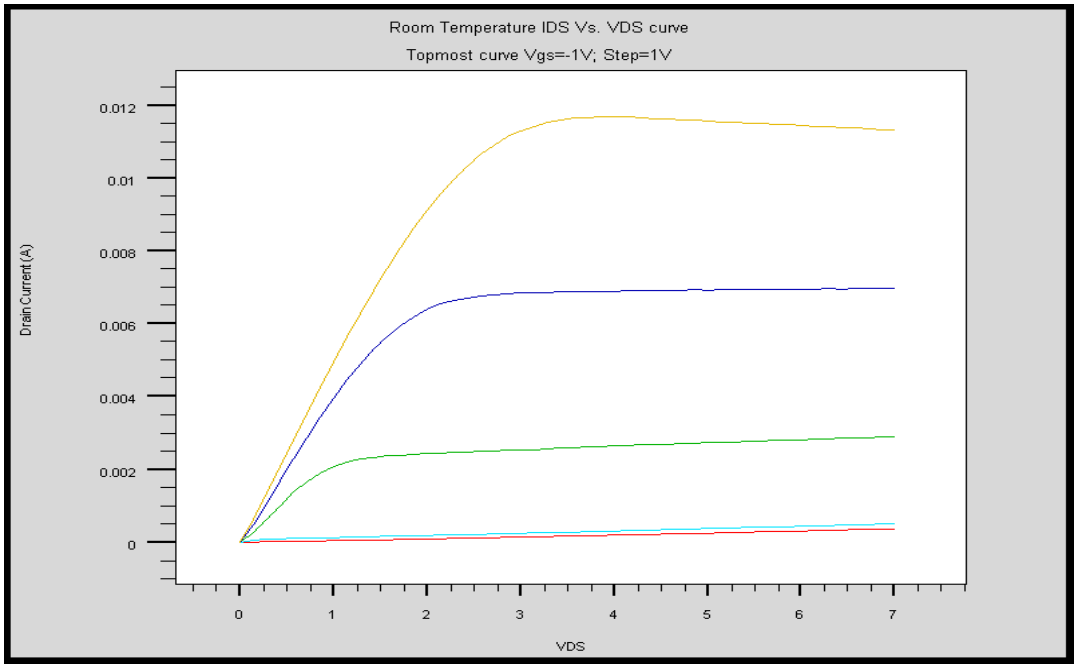

Figure 18: Measured Berkeley HEMT Device I-V Characteristic.

The two I-V characteristic curves match closely with a few exceptions. The topmost curve on the modeled device peaks at about 14 mA while the topmost curve on the physical device peaks at about 12 mA. The topmost curve on the physical device has a negative slope in the saturation region attributed to a negative resistance due to the poor thermal qualities of sapphire. I was unable to match the negative going slope on the modeled device. Although thermal effects were added to the device model, the combination used in this effort did not produce the exact results. The I-V characteristics match closely enough to give me confidence that the device was modeled correctly and it can be used to conduct follow on thermal measurements.

C. THERMAL CHARACTERIZATION

The majority of the modeling efforts in this thesis have been dedicated to ensuring that there was a proper HEMT device model to be used for thermal testing. The previous sections have demonstrated that the HEMT device modeled is a good representation of the Berkeley device when modeled at room temperature. This section will analyze the

model characteristics over a range of temperatures and compare the simulation results to the measured results of the physical device over the same range.

1. Physical Device Thermal Testing

The thermal testing for the physical device was conducted utilizing the UTMOST™ program and a hot chuck on the Micromanipulator testing microscope. The physical device was tested at room temperature, 100º C, 200º C, and 300º C. Figure 19 is a compilation of the I-V characteristics over the range of temperatures.

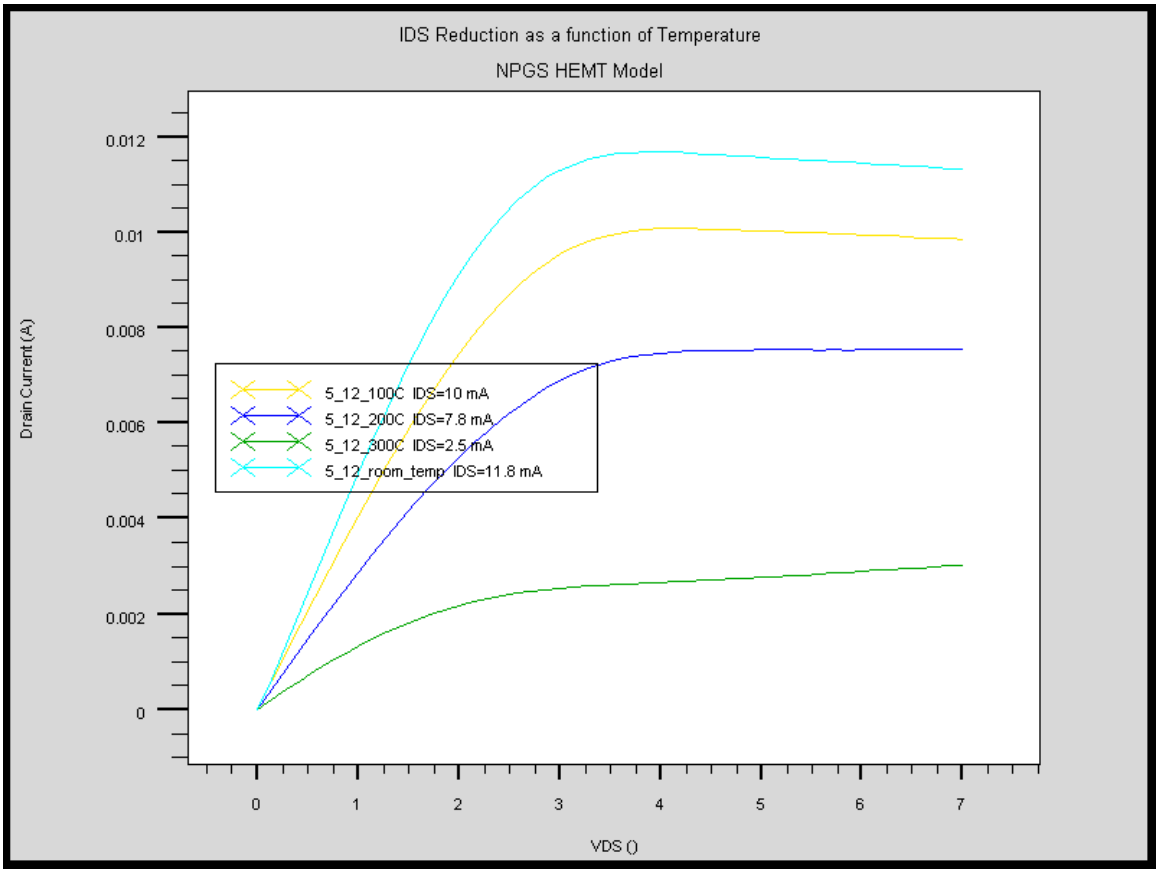

Figure 19: Topmost Curve (V_{gs}= -1 V) I-V Measurement of Physical Device over a range of temperatures.

Figure 20, Figure 21, and Figure 22 represent the I-V characteristic of the room temperature measurement against 100ºC, 200ºC, and 300ºC respectively. The figures clearly show the current degradation due to the temperature increase.

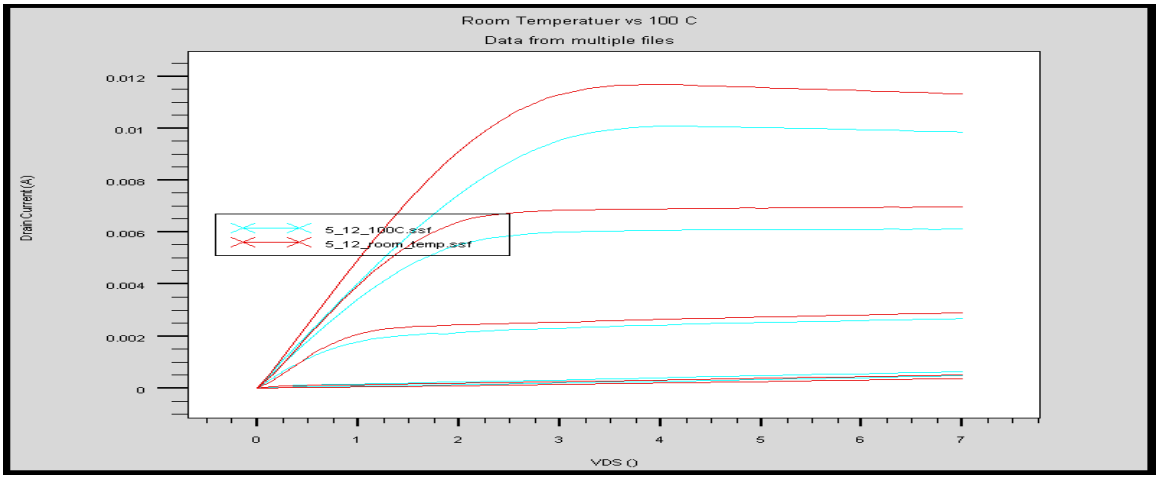

Figure 20: I-V Characteristic Room Temperature vs. 100º C.

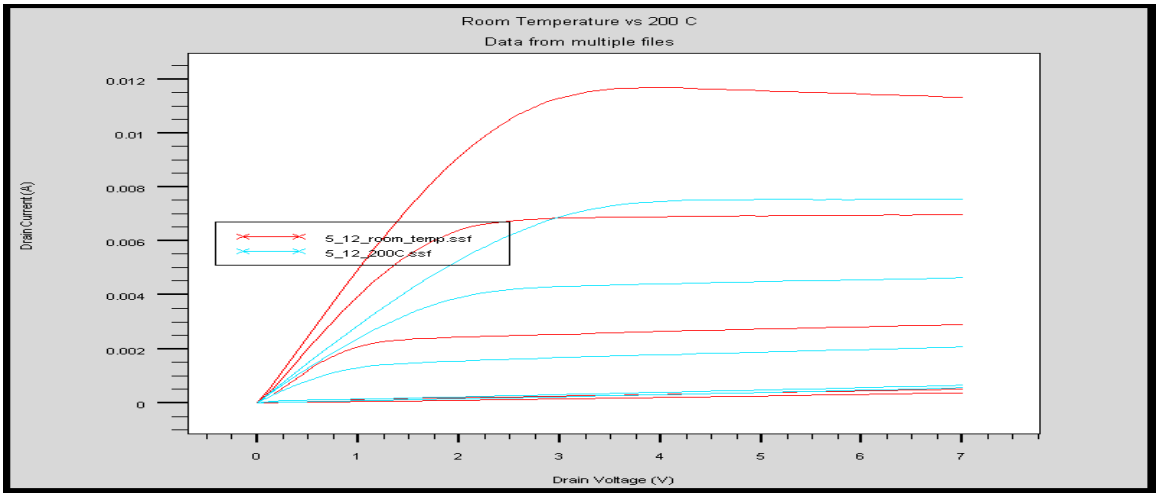

Figure 21: I-V Characteristic Room Temperature vs. 200º C.

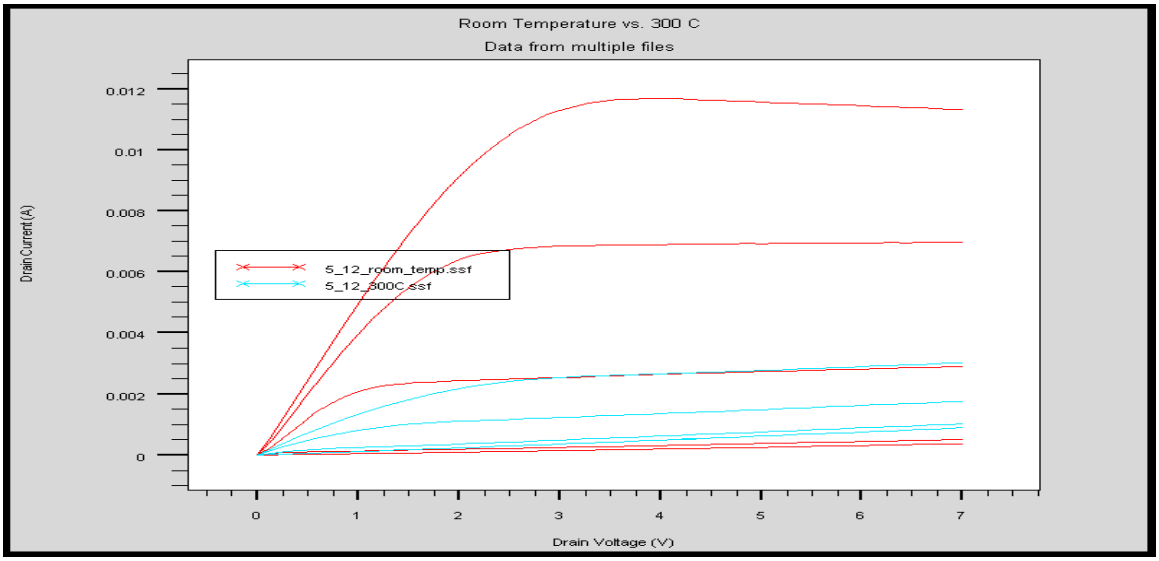

Figure 22: I-V Characteristic Room Temperature vs. 300º C.

Testing the physical device over a range of temperatures served as the starting point for the thermal model development. Utilizing the data gained from the physical devices, the simulated device was modified to simulate lattice heating. The GIGA™ routine was utilized in the thermal testing of the device model and will be discussed in section two of this chapter.

2. NPS HEMT Model Thermal Testing

Introducing the thermal characteristics of a HEMT device is accomplished through the GIGA™ routine. GIGA™ extends ATLAS™ to account for lattice heat flow and general thermal environments [16]. The models included in this device (see Appendix A) were the lat.temp model and the joule.heat model. These two models enable ATLAS™ to apply heat flow equations to the solution of the device parameters. To simulate the hot chuck in the physical device testing, a thermal contact was placed in the substrate and set to the desired temperature. This applied the same temperature to the model as the hot chuck applied to the actual device. The purpose of this type of testing was to ensure that the HEMT model would react in the same manner as the physical device did when heated. The results, although not exactly the same, were remarkably similar and indicated that the modeled device reacted similar to the physical device under thermal stress. The following figures are of the HEMT model I-V characteristics under

the same thermal environment the physical devices were subjected to. Figure 23, Figure 24, and Figure 25 represent the model I-V characteristics over temperature.

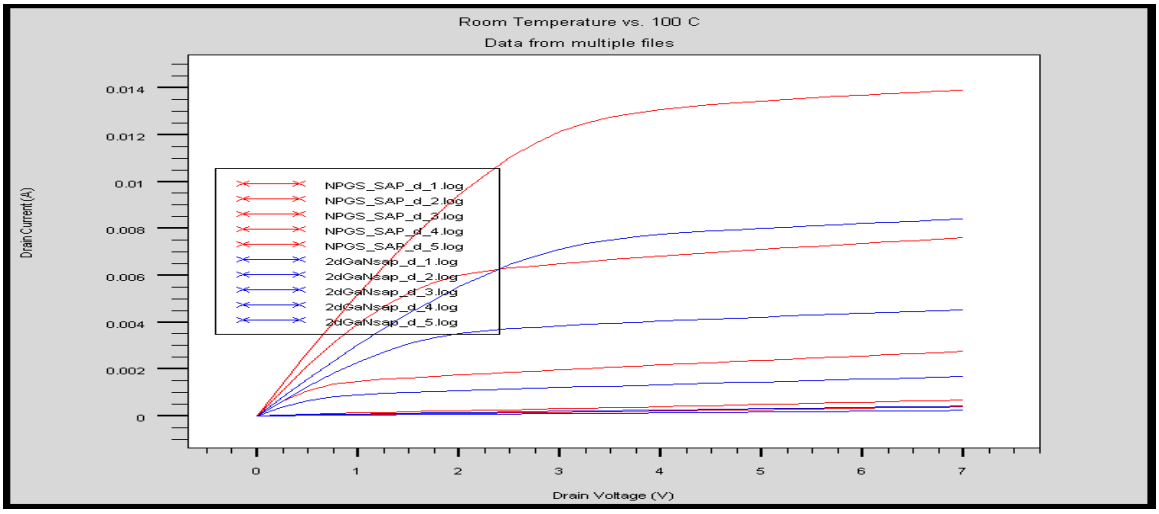

Figure 23: NPS HEMT Room Temperature vs. 100º C.

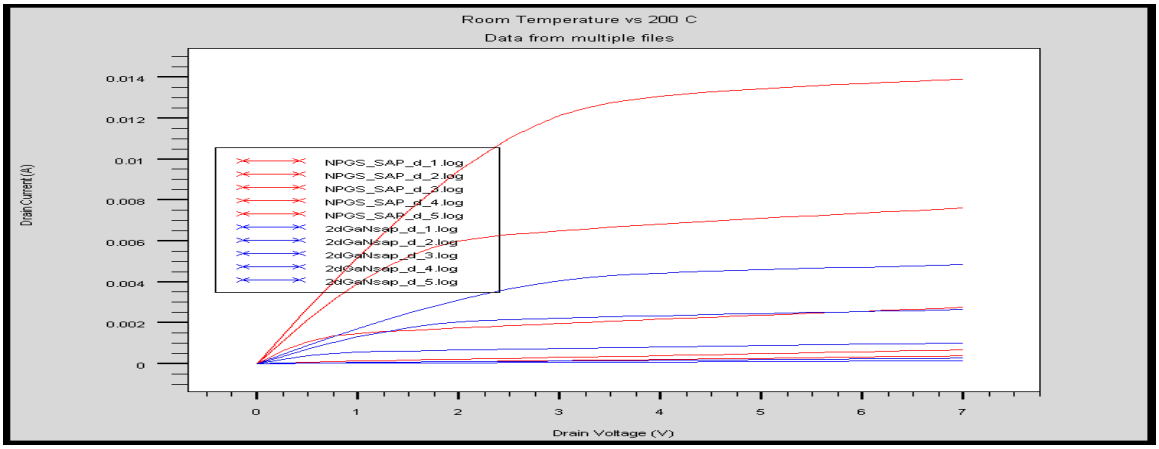

Figure 24: NPS HEMT Room Temperature vs. 200º C.

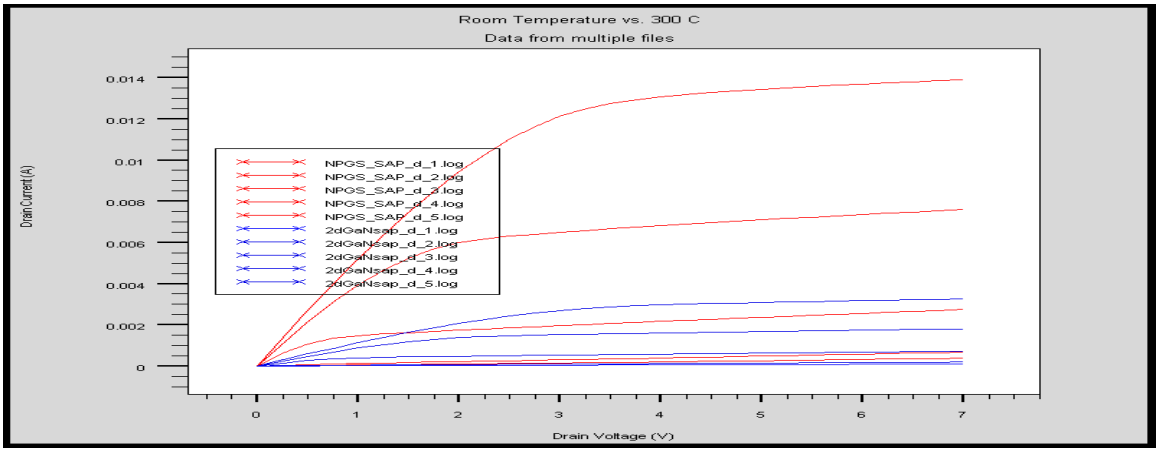

Figure 25: NPS HEMT Room Temperature vs. 300º C.

The I-V characteristics of the model show the same general trend as the physical device. Table 4 shows the differences in the model and physical device. The error analysis is conducted on the topmost curve which represents a gate voltage of -1 V.

	Room Temperature	100º C	200º C	300º C
Physical Device	0.012 A	0.01 A	0.007 A	0.002 A
Percent Change		16.6%	41.6%	83%
Modeled Device	0.014 A	0.009 A	0.004 A	0.002 A
Percent Change		35.7%	71.4%	83%

Table 4: Percent Reduction in Current with Temperature.

Although the percent change is approximately double in the model design, the same general decreasing current trend is observed in the modeled device. The trend indicates that the thermal models incorporated in the HEMT model are within a factor of 2 of degradation, and should be sufficient to investigate thermal testing. Figure 26 illustrates the decreasing current trend as the lattice temperature of the device is increased from room temperature to 300° C.

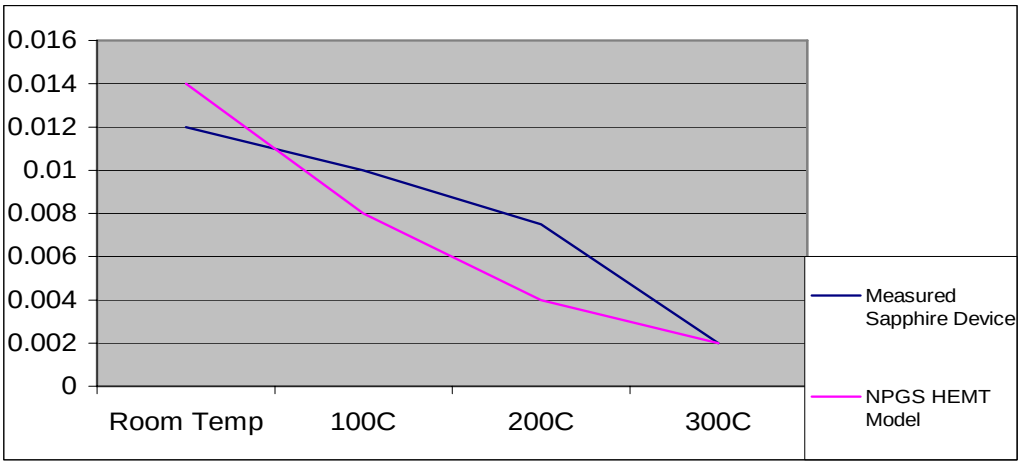

Figure 26: Decreasing Current trend of Actual Device and Modeled Device.

An important measure utilized in high power electronic FET devices is gate leakage. When the device as previously described, there is a significant shift in the gate leakage. Figure 27 illustrates an approximate increase of four orders of magnitude in gate leakage per 100° C.

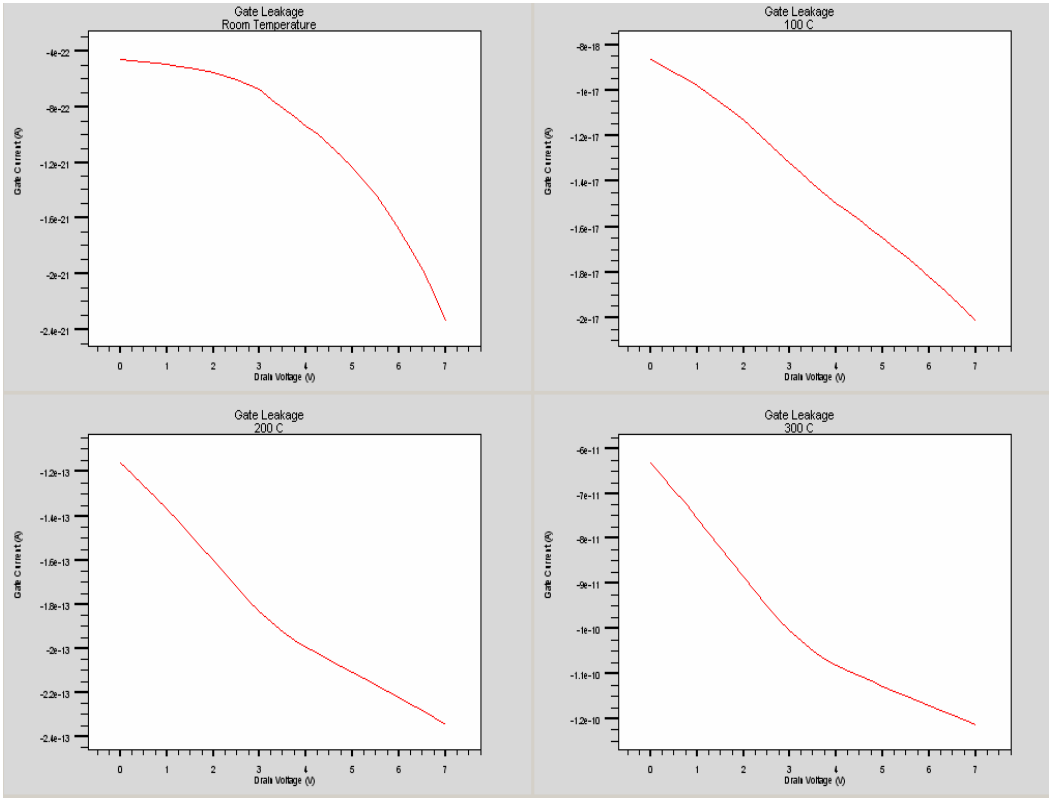

Figure 27: NPS HEMT Gate Leakage Over Temperature.

D. FINAL THERMAL SIMULATION

The final thermal simulation will consist of running the HEMT model at a high DC bias which will result in high temperatures required to analyze a change in substrate materials. To accomplish the shift in from sapphire to diamond substrate materials, the thermal conductivity constant tc.a was set to 0.1 for a thermal conductivity of 10 and 0.05 for a thermal conductivity of 20. The values for thermal conductivity were taken from [18], the SP3 corporation website. SP3 is working with NPS and UC Berkeley to develop diamond substrates suitable for AlGaN/GaN HEMT development. The device will be biased as described in the previous section except the drain will be swept from 0 to 55V.

1. Sapphire vs. Diamond Substrate Comparison

The point of testing the HEMT device on different substrates was to determine if a change in substrate material will reduce the channel temperature. Once a suitable HEMT device was modeled, it was swept from zero to 55 V on the drain creating a high current situation. The result of the higher drive current was increased channel/device temperature. Figure 28 shows a contour plot of the device on sapphire and diamond substrates indicating the lattice temperature throughout the device. The thermal conductivity of diamond ranges between 10 and 20, Figure 28 represents diamond thermal conductivity set to 10 and sapphire thermal conductivity set to 1.7.

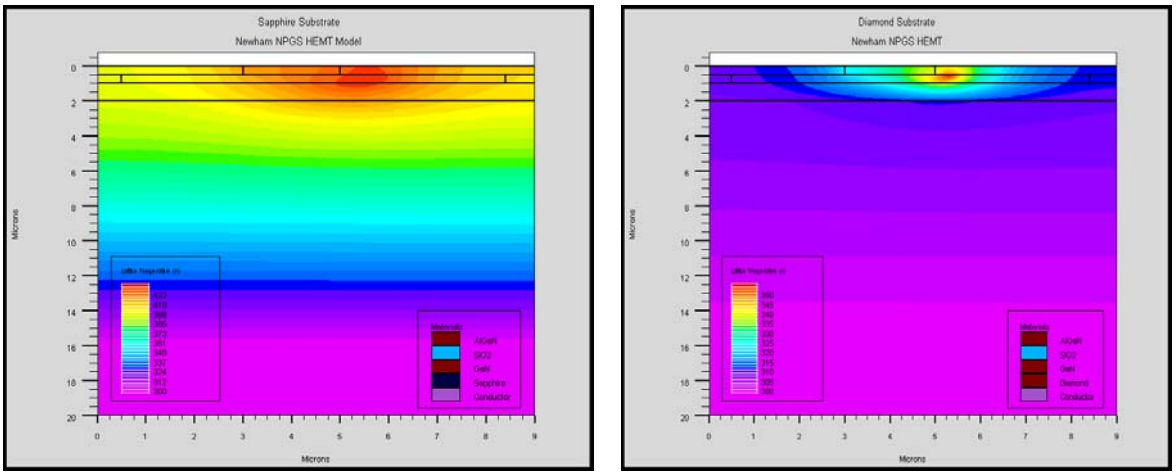

(a) **(b)**

Figure 28: Contour Plot of (a) Sapphire Substrate Material and (b) Diamond Substrate.

The plot indicates that the peak temperature in the device changes dramatically with a change in substrate material. Of particular note, the diamond substrate device was able to dissipate more heat per unit area, and the size of the "hot spot" was reduced by approximately 75%. The sapphire substrate device under the 55 V drain bias reached a maximum temperature of 157ºC while the diamond substrate device reached a temperature of 84º C. Figure 30 shows a drain current of approximately 0.06 A/mm for the diamond substrate device with a TC constant of 20. With 55 V applied to the drain of the device, the output power of the modeled device was calculated to be 3.3 W/mm.

Figure 29 is a plot taken from a horizontal cutline along the 2DEG of the sapphire substrate device, the diamond substrate device with a thermal conductivity constant of 10 and 20. Although the simulation was conducted with varying diamond thermal conductivities, the results indicate that the model is relatively insensitive to the thermal conductivity change of diamond. There was a 2% change in channel temperature and an 8% change in drain current. The peak temperature of the device remained the same when the thermal conductivity was changed from 10 to 20.

Figure 29 better illustrates the advantage the diamond substrate provides. The area under each of the thermal curves represents the average temperature of the channel. The average channel temperature of the sapphire substrate device is 137ºC, the diamond substrate with a thermal conductivity parameter of 10 reduced the average channel temperature to 47ºC, and the diamond substrate with a thermal conductivity parameter of 20 reduced the average channel temperature to 46ºC. The average channel temperature was calculated utilizing the integrate function of TONYPLOT™. The simulation indicates that a dramatic reduction in lattice temperature and channel temperature occurs by changing the substrate material from sapphire to diamond.

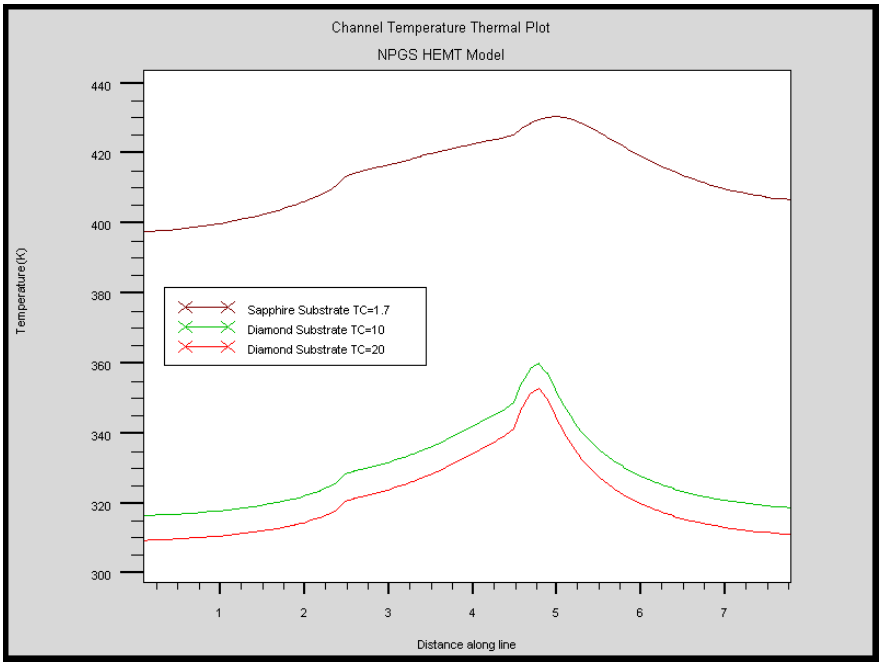

Figure 29: Thermal Horizontal Cutline of 2DEG with Diamond Thermal Conductivity set to 10 and 20. Sapphire (brown) Diamond 10 (green) and Diamond 20 (red).

Figure 30 shows the device drain current utilizing the three different substrates.

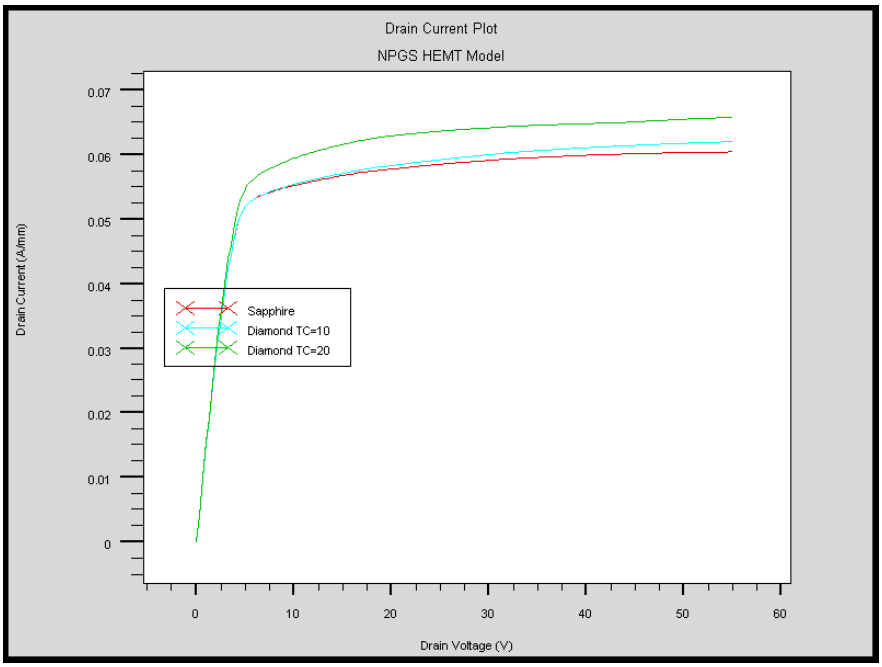

Figure 30: Drain Current as a Function of Substrate Material.

The final parameter to be analyzed is the change in the gate leakage characteristic with a change in substrate material. Figure 31 illustrates the gate leakage characteristic as a function of substrate material.

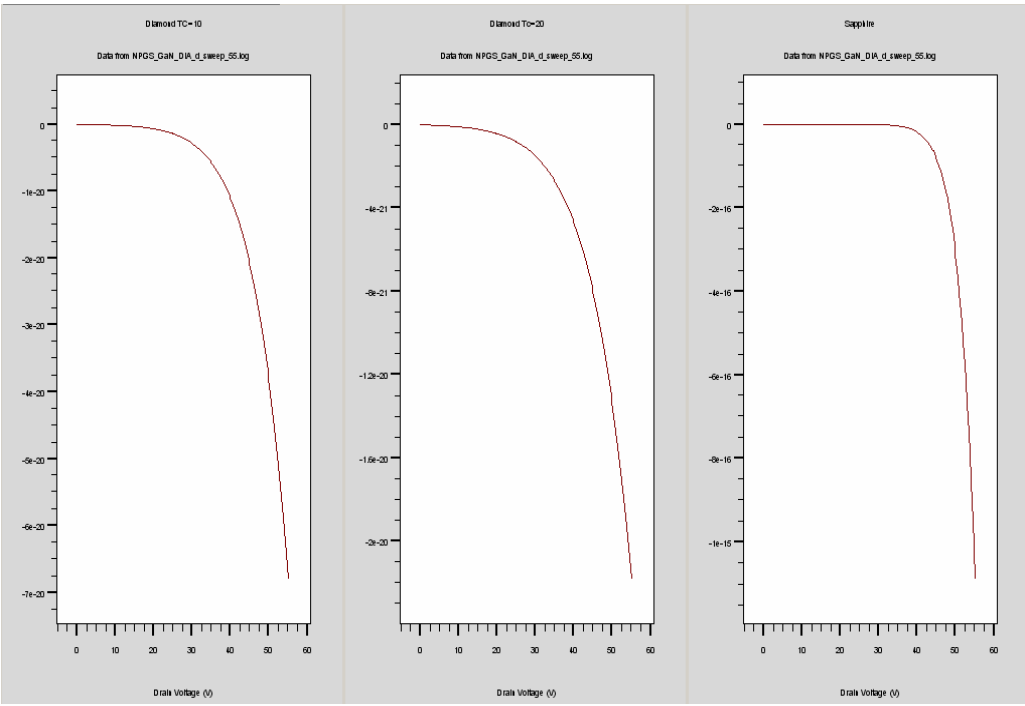

Figure 31: Gate Leakage as a Function of Substrate Material.

There is a reduction of five orders of magnitude in the amount of gate leakage on the diamond substrate device compared to the sapphire substrate device. Every measure of effectiveness of a HEMT device improved with a change in substrate material. The simulation indicates that HEMT devices grown on diamond substrates will improve the overall effectiveness of the device when high power applications are required. Although it is beyond the scope of this thesis, it is logical to assume that the reliability of the devices will be enhanced if the temperature can be reduced.

Table 5 shows the results of the various parameters tested. The change was calculated with the diamond TC=10 parameter.

	Diamond TC=10	Diamond TC=20	Sapphire	Change
Peak Temperature	84 C	84 C	150 C	56%
Channel Temperature	47 C	46 C	137 C	34%
Gate Leakage	7.00E-20	2.00E-20	1.00E-15	1E5
Drain Current	.57 A	.62 A	.55 A	0.04%

Table 5: Summary of Testing Results.

E. CHAPTER CONCLUSION

This chapter introduced the modeling techniques utilized to simulate the AlGaN/GaN HEMT device. To ensure proper thermal modeling a HEMT model was developed and tested both at room temperature and at various temperatures. The results of the model were compared with the physical device for accuracy. Once a suitable device structure was developed, it was subjected to a high bias condition to generate internal heating. The device parameters were then extracted from a sapphire based substrate and then a diamond substrate to determine if the substrate material enhanced the thermal capacity of the device. It was shown that a diamond substrate has a dramatic effect on channel temperature. There was a 54% reduction in peak temperature and a 34% reduction in the channel temperature. The following chapter briefly summarizes the work completed on this thesis and will make recommendations for follow-on simulations.

THIS PAGE INTENTIONALLY LEFT BLANK

IV. CONCLUSIONS AND RECOMMENDATIONS

A. CONCLUSIONS

The AlGaN/GaN HEMT model developed in this thesis provides a representation of an actual HEMT device that was tested over a range of temperatures from 27^0C to 300^0C and validated against measured data. The thermal effects that occur by device self heating effects were correctly modeled through the Silvaco's GIGA™ routine. The HEMT model was able to duplicate the actual transistor operation both electrically and thermally. The I-V curves generated by the software model represented the actual device I-V curves well with only a 13% difference at the topmost I-V curve.

The difficult part of this thesis was ensuring that a proper HEMT device was modeled. A tremendous effort was made ensuring all operational aspects of the HEMT device were addressed. The focus of the thesis however, was to examine the thermal effects of the device when the substrate material was changed from sapphire to diamond. Changing the substrate and examining the thermal properties was accomplished by changing the material name in the ATLAS™ file and adjusting the thermal conductivity constants. Sapphire's thermal conductivity was set to 1.7 W/cm·K, and diamond's thermal conductivity was set to both 10 and 20 W/cm·K to test over the range given by SP3 incorporated. The effects of the substrate change were drastic. There was a 1/2 reduction in the peak temperature of the device when diamond was used see Table 5. The average temperature in the channel was reduced by 1/3. Thermal analysis is important in the calculation of device lifetime. One approach to predicting device median lifetimes is the Arrhenius model for temperature dependence [4] and is given by:

$$t_m(T) = Ae^{\frac{E_A}{kT}} \tag{4.1}$$

where EA is the activation energy (eV), A is a constant acceleration factor (dimensionless) and k is the Boltzmann's constant (eV/T). Activation energies range from 0.3 eV to 1.7 eV for GaN HEMTs [7]. Utilizing an acceleration factor of 1 and

activation energy of 0.3 eV and 1.7 eV, the median lifetime of a HEMT device can theoretically be increased to a range of 5 to 1e6 times the median lifetime of a sapphire substrate HEMT.

Initially, I attempted to utilize the new polarization models available in ATLAS™. Many attempts to model the polarization effects by utilizing the PSP and POLARIZATION statements failed. I was unable to get a suitable bangap diagram or 2DEG utilizing the new BLAZE™ models. The interface statement on the AlGaN side of the heterojunction provided the best method to simulate the polarization effects experienced in wurtzite materials. The interface command places a sheet charge at the interface and provides the necessary electron concentration to form the 2DEG.

The model designed in this thesis proved to be relatively insensitive to the thermal conductivity constants given for diamond. There was very little change in any of the parameters analyzed when the constants were varied through the published values. Although many factors in the ATLAS™ code had to be optimized to get a representative HEMT device, one of the enabling parameters to simulate a geometrically correct device was the Albrecht model. Albrecht *et al.* [19] developed a set of transport parameters for devices with electron conduction GaN (position of the 2DEG). The Albrecht parameter models the carrier mobility as a function of doping and lattice temperature which are critical parameters in the device modeled for this thesis. In [19] Albrecht provides initial experimental values for the variables available in the ATLAS™ model. These values were implemented in the HEMT model and then optimized to match the measured device characteristics. The variables in the Albrecht model proved to be the most sensitive parameters affecting the I-V curves and further analysis and optimization efforts should provide a better I-V representation.

B. RECOMMENDATIONS

Follow-on efforts should examine the possibility of implementing the polarization and piezoelectric models available in ATLAS™ to determine if a suitable model can be developed utilizing the new polarization models.

The parameters examined in this thesis were DC measurements only. One of the advantages of a HEMT is that it has the ability to operate at high frequencies. It would be beneficial to examine the RF characteristics of the model developed in this thesis to see if the modeled device can accurately simulate the RF parameters of an actual HEMT device. Once the basic characteristics are extracted, the device should be simulated at high-frequency, high-power conditions to determine if the benefits of a diamond substrate are as dramatic in the AC domain.

The HEMT design presented utilized an 18μm thick sapphire or diamond substrate. The purpose of simulating the model with a thick substrate was to analyze the thermal parameters when the device was not saturated thermally. The assumption in this model is that the device is capable of dissipating all of the heat applied. In reality, the substrate thickness will be much smaller and a more comprehensive heat flow study should be conducted in order to simulate a more realistic environment.

The two dimensional analysis of the device provided and adequate simulation of the HEMT device, however Silvaco has a three dimensional capability that can provide a more comprehensive analysis of the device operational parameters. The model developed in this thesis can be expanded to a three dimensional model in order to re-examine the electrical and thermal properties of the device. An initial attempt was made to extend the model to three dimensions, but I was unable to get the model to converge at a high bias condition. The probable cause of the failure was meshing techniques. Great care must be taken to properly mesh the device for simulation. In three dimensions, the number of nodes required for a solution increases dramatically. If there are too many nodes, the computation time is prohibitively long, and if the mesh is reduced too much, the results will not be accurate.

The physical device grown on a sapphire substrate tested for this thesis was designed and fabricated by S. Tzeng at UC Berkeley. The Weber material science group at UC Berkeley, NPS, and SP3 are currently working to grow AlGaN/GaN HEMT devices on diamond substrates. Once a viable diamond substrate device is created, a comprehensive test should be preformed on the device to see if the ATLAS™ model accurately predicts the thermal effects of the diamond substrate device. Once the

diamond HEMTs are available and tested to ensure model accuracy, electrical defect densities could be modeled to increase with temperature. A study could be performed to predict degradation due to temperature and time. The initial results gained from this thesis indicate that AlGaN/GaN HEMTs grown on a diamond substrate have the possibility to be the enabling technology for high-power high-frequency operations.

LIST OF REFERENCES

1. F. Ren and J. C. Zolper, *Wide Energy Bandgap Electronic Devices.* River Edge, NJ: World Scientific Publishing Co. Pte. Ltd., 2003, pp. 514.

2. E. J. Martinez, "Gallium Nitride & Related Wide Bandgap Materials and Devices," pp. 17, 2005.

3. J. A. Mittereder, S. C. Binari, P. B. Klein, J. A. Roussos, D. S. Katzer, D. F. Storm, D. D. Koleske, A. E. Wickenden and R. L. Henry, "Current collapse induced in AlGaN/GaN HEMTs by short-term DC bias stress," in 2003, pp. 320-323.

4. F. Jensen. 1995, *Electronic Component Reliability.*

5. K. P. Eimers, "2-D Modeling of GaN HEMTs Incorporating the Piezoelectric effect." *Master's Thesis, Naval Postgraduate School, Monterey, California,* 2001.

6. K. L. Holmes. 2002, Two-dimensional modeling of aluminum gallium nitride. *Master's Thesis, Naval Postgraduate School, Monterey, California*

7. R. P. Salm. 2005, Thermal modeling of GaN HEMTs on sapphire and diamond. *Master's Thesis, Naval Postgraduate School, Monterey, California.*

8. J. C. Freeman. 2003, Basic equations fro the modeling of gallium nitride (GaN) high electron mobility transistors (HEMTs). *NASA/TM--2003-211983* Available: http://gltrs.grc.nasa.gov/reports/2003/TM-2003-211983.pdf

9. S. Tzeng, "Low-Frequency Noise Sources in III-V Semiconductor Heterostructures," 2004.

10. P. Javorka, "Fabrication and Characterization of AlGaN/GaN High Electron Mobility Transistors." 2004.

11. S. M. Sze, *Modern Semiconductor Device Physics.* New York: John Wiley & Sons, Inc., 1998, pp. 556.

12. R. F. Pierret, *Semiconductor Device Fundamentals.* Massachusetts: Addison Wesley Longman, 1996, pp. 792.

13. M. Lundstrom, *Fundamental of Carrier Transport.* ,2nd ed.New York: Cambridge University Press, 2000, pp. 418.

14. P. Valizadeh and D. Pavlidis, "Investigation of the impact of Al mole-fraction on the consequences of RF stress on Al/sub x/Ga/sub 1-x/N/GaN MODFETs," *Electron Devices, IEEE Transactions on,* vol. 52, pp. 1933-1939, 2005.

15. O. Ambacher, B. Foutz, J. Smart, J. R. Shealy, N. G. Weimann, K. Chu, M. Murphy, A. J. Sierakowski, W. J. Schaff, L. F. Eastman, R. Dimitrov, A. Mitchell and M. Stutzmann, "Two dimensional electron gases induced by spontaneous and piezoelectric polarization in undoped and doped AlGaN/GaN heterostructures," *J. Appl. Phys.*, vol. 87, pp. 334-344, 01/01/. 2000.

16. Silvaco International, "Silvaco International, ATLAS User's Manual, February 2000." 2000.

17. I. P. Smorchkova, C. R. Elsass, J. P. Ibbetson, R. Vetury, B. Heying, P. Fini, E. Haus, S. P. DenBaars, J. S. Speck and U. K. Mishra, "Polarization-induced charge and electron mobility in AlGaN/GaN heterostructures grown by plasma-assisted molecular-beam epitaxy," *J. Appl. Phys.*, vol. 86, pp. 4520-4526, 10/15/. 1999.

18. SP3 Incorporated. Available: http://www.sp3inc.com/

19. J. D. Albrecht, R. P. Wang, P. P. Ruden, M. Farahmand and K. F. Brennan, "Electron transport characteristics of GaN for high temperature device modeling," *J. Appl. Phys.*, vol. 83, pp. 4777-4781, 05/01/. 1998.

APPENDIX: ATLAS™ INPUT DECK

```
##########################################################################
##########################################################################
#LT Scott Newham
#NPS AlGaN/GaN HEMT Design
#
#267 Angstrom AlGaN layer
# Schottky WF=4.3
# 1e15 doping GaN AlGaN=1e10
#Interface charge=.99e13
# no doping in AlGaN
# Albrct mobility model an.albrct=5e-3 bn.albrct=3e-3 cn.albrct=2e-3
##########################################################################
go atlas
set devthk=20
set sourcegatespace=2
set gatedrainspace=3
set devwidth=4+$sourcegatespace+$gatedrainspace
set reg3xmin=$devwidth-1
set reg4xmin=1+$sourcegatespace
set reg4xmax=2+$reg4xmin
set reg5xmax=$devwidth-.5
set drainxmin=$devwidth-1
set drainxmax=$devwidth-.6
set ifchargemax=$devwidth-1.05
set WF=4.3
# Sweep increment
set vstart = 0
set vstop = 7
set vinc = .25
#################### Mesh Construction #############
####Mesing and width = 100 microns#################
mesh auto width=100
x.m l=0.0 s=0.1
x.m l=0.5 s=0.1
x.m l=1.0 s=0.1
x.m l=$reg4xmin s=0.1
x.m l=$reg4xmax s=0.1
x.m l=$reg3xmin s=0.1
x.m l=$reg5xmax s=0.1
x.m l=$devwidth s=0.1
y.m l=0 s=0.5
y.m l=0.4 s=0.1
y.m l=0.49 s=0.005
y.m l=0.5 s=0.005
y.m l=0.525 s=0.005
y.m l=0.5267 s=0.00005
y.m l=0.5269 s=0.00005
y.m l=0.5270 s=0.005
y.m l=1.0 s=0.1
y.m l=2 s=0.5
y.m l=$devthk s=2.0
######################### Region Definitions ################

region num=1 mat=AlGaN donors=1e10 x.comp=0.28 x.min=0.5 x.max=$reg5xmax
y.min=0.5 y.max=0.5267
region num=2 mat=oxide x.min=0 x.max=$devwidth y.min=0 y.max=0.5
region num=3 mat=GaN donors=1e15 x.min=0.5 x.max=$reg5xmax y.min=0.5267
y.max=0.5269
```

```
region num=4 mat=GaN donors=1e15 x.min=0.5 x.max=$reg5xmax y.min=0.5269
y.max=1.0
region num=5 mat=GaN donors=1e15 x.min=0 x.max=$devwidth y.min=1 y.max=2
region num=6 mat=Sapphire x.min=0 x.max=$devwidth y.min=2 y.max=$devthk
elec num=1 name=source x.min=0 x.max=0.5 y.min=0.5 y.max=1
elec num=2 name=drain x.min=$drainxmax x.max=$devwidth y.min=0.5 y.max=1
elec num=3 name=gate x.min=$reg4xmin x.max=$reg4xmax y.min=0 y.max=0.5
elec num=4 substrate

############### Modifying Statements ##################
########Inserts polarization effects########
interface charge=0.99e13 y.min=.52 y.max=.5267 s.s

material mat=AlGaN align=.8
mobility albrct.n an.albrct=5e-3 bn.albrct=3e-3 cn.albrct=2e-3 vsatn=2e7
material mat=GaN tcon.polyn
material mat=AlGaN tcon.polyn
material mat=Sapphire tcon.polyn
models k.p print lat.temp joule.heat srh albrct
contact name=gate work=$WF

#thermcontact num=1 x.min=0 x.max=$devwidth y.min=2 y.max=5 temp=300 ^boundary
alpha=1.7
thermcontact num=1 x.min=0 x.max=$devwidth y.min=14 y.max=$devthk temp=300
^boundary alpha=1.7
output con.band val.band charge
method gumits=300 clim.dd=1e5 autonr block carr=1
######################## Output Statements ###########
# idvd curves
solve
save outf=NPGS_SAP_g0.str
log outf=NPGS_SAP_d_0.log
solve name=drain vdrain=$vstart vfinal=$vstop vstep=$vinc
save outf=NPGS_2D_SAP_g0d7.str
log off
tonyplot NPGS_SAP_d_0.log -set IDVD.set
solve vdrain=0 vgate= -5
save outf=solve_vgate-5.str
log outf=NPGS_SAP_d_1.log
solve name=drain vdrain=$vstart vfinal=$vstop vstep=$vinc
log off
solve vdrain=0 vgate= -4
save outf=solve_vgate-4.str
log outf=NPGS_SAP_d_2.log
solve name=drain vdrain=$vstart vfinal=$vstop vstep=$vinc
log off
solve vdrain=0 vgate= -3
save outf=solve_vgate-3.str
log outf=NPGS_SAP_d_3.log
solve name=drain vdrain=$vstart vfinal=$vstop vstep=$vinc
log off
solve vdrain=0 vgate= -2
save outf=solve_vgate-2.str
log outf=NPGS_SAP_d_4.log
solve name=drain vdrain=$vstart vfinal=$vstop vstep=$vinc
log off
solve vdrain=0 vgate= -1
save outf=solve_vgate-1.str
log outf=NPGS_SAP_d_5.log
solve name=drain vdrain=$vstart vfinal=$vstop vstep=$vinc
log off
#solve vdrain=0 vgate= 0
#save outf=solve_vgate_0.str
```

```
#log outf=NPGS_SAP_d_6.log
#solve name=drain vdrain=$vstart vfinal=$vstop vstep=$vinc
#log off
#solve vdrain=0 vgate= 1
#save outf=solve_vgate_1.str
#log outf=NPGS_SAP_d_7.log
#solve name=drain vdrain=$vstart vfinal=$vstop vstep=$vinc
#log off
tonyplot NPGS_SAP_d_0.log -overlay NPGS_SAP_d_1.log -overlay NPGS_SAP_d_2.log -
overlay NPGS_SAP_d_3.log -overlay NPGS_SAP_d_4.log -overlay NPGS_SAP_d_5.log -\
overlay NPGS_SAP_d_6.log -overlay NPGS_SAP_d_7.log -set IDVD.set
# idvg curve
#log outf=NPGS_GaNsapp-gate_sweep.log
#solve vdrain=0
#solve name=gate vgate=0 vfinal=-4.2 vstep=.6
quit
```

THIS PAGE INTENTIONALLY LEFT BLANK

INITIAL DISTRIBUTION LIST

1. Defense Technical Information Center
   Ft. Belvoir, Virginia

2. Dudley Knox Library
   Naval Postgraduate School
   Monterey, California

3. Engineering and Technology Curricula Office, Code 34
   Naval Postgraduate School
   Monterey, California

4. Chairman, Code EC (590)
   Department of Electrical and Computer Engineering
   Naval Postgraduate School
   Monterey, California

5. Professor Todd R. Weatherford, Code EC(590)/Wt
   Department of Electrical and Computer Engineering
   Naval Postgraduate School
   Monterey, California

6. Andrew A. Parker, Code EC(590)/Pk
   Department of Electrical and Computer Engineering
   Naval Postgraduate School
   Monterey, California\

7. Dr. Petra Specht
   Materials Science and Engineering
   University of California, Berkeley at LBNL
   Berkeley, California

8. Jerry Zimmer
   SP3 Diamond Technologies
   Santa Clara, California

9. LT Wesley S. Newham, United States Navy
   Salinas, California